Geophysical Journal International

Geophys. J. Int. (2017) **208,** 403–423
Advance Access publication 2016 November 2
GJI Geodynamics and tectonics

doi: 10.1093/gji/ggw407

Investigating the architecture of the Paganica Fault (2009 M_w 6.1 earthquake, central Italy) by integrating high-resolution multiscale refraction tomography and detailed geological mapping

F. Villani,[1] L. Improta,[2] S. Pucci,[2] R. Civico,[2] P.P.G. Bruno[3] and D. Pantosti[2]

[1] *Istituto Nazionale di Geofisica e Vulcanologia, via dell'Arcivescovado* 8 – *I*-67100 *L'Aquila, Italy. E-mail: fabio.villani@ingv.it*
[2] *Istituto Nazionale di Geofisica e Vulcanologia, via di Vigna Murata,* 605 – *I*-00143 *Roma, Italy*
[3] *The Petroleum Institute, Petroleum Geoscience Dept., PO Box* 2533, *Abu Dhabi, UAE*

Accepted 2016 October 31. Received 2016 September 29; in original form 2016 June 15

SUMMARY

We present a 2-D subsurface image of the Paganica Fault from a high-resolution refraction tomography and detailed geological investigation carried out across part of the northwestern segment of the 20-km-long Paganica–San Demetrio fault-system, and which was responsible of the 2009 April 6 M_w 6.1 L'Aquila earthquake (central Italy). We acquired two seismic profiles crossing the Paganica basin with a dense-wide aperture configuration. More than 30 000 *P* wave first-arrival traveltimes were input to a non-linear tomographic inversion. The obtained 250–300 m deep 2-D *Vp* images illuminate the shallow portion of the Paganica Fault, and depict additional unreported splays defining a complex half-graben structure. We interpret local thickening of low-*Vp* (<2400 m s^{-1}) and intermediate-*Vp* (2600–3400 m s^{-1}) regions as syn-tectonic clastic wedges above a high-*Vp* (3800–5000 m s^{-1}) carbonate basement. These results are condensed in a 4.2-km-long section across the Paganica basin, clearly indicating that the Paganica Fault is a mature normal fault cutting the whole upper ∼10 km of the crust. We evaluate a minimum cumulative net displacement of 650 ± 90 m and a total heave of 530 ± 65 m accomplished by the Paganica Fault, respectively. In the conservative hypothesis that the extension started during the Gelasian (1.80–2.59 Ma), we obtain a minimum long-term slip-rate of 0.30 ± 0.07 mm yr^{-1} and an extension-rate of 0.25 ± 0.06 mm yr^{-1}, respectively. Considering the regional averaged extensional field of ∼1 mm yr^{-1} obtained from geodetic and geological analyses at 10^4 yr timescale, we infer that the Paganica Fault accounts for ∼20 per cent of the NE-extension affecting this zone of the central Apennines axis due to the concurrent activity of other parallel normal fault-systems nearby (e.g. the Liri, Velino-Magnola, L'Aquila-Celano and Gran Sasso fault-systems).

Key words: Palaeoseismology; Seismicity and tectonics; Seismic tomography; Continental neotectonics; Fractures and faults; High strain deformation zones.

1 INTRODUCTION

The central Apennines of Italy are a Neogene fold-and-thrust belt (Malinverno & Ryan 1986; Cosentino *et al.* 2010; Vezzani *et al.* 2010) where post-orogenic extension takes place since the Late Pliocene–Early Pleistocene (Lavecchia *et al.* 1994; Cavinato & De Celles 1999; Ghisetti & Vezzani 1999; D'Agostino *et al.* 2001). This region is characterized by one of the highest seismic releases in the Mediterranean area, mostly due to crustal earthquakes of normal-faulting type and magnitude occasionally up to ∼6.5–7. The extending belt is ∼50–80 km wide and is parallel to the topographic bulge of the chain (Fig. 1; Chiarabba & Chiodini 2013): here, the current extensional regime is evidenced by (1) focal mechanisms of shallow (∼5–15 km deep) earthquakes (Chiarabba *et al.* 2005; Pondrelli *et al.* 2006; Bagh *et al.* 2007), (2) borehole breakout analyses (Montone *et al.* 2012) and (3) geodetic data indicating regional extension rates on the order of ∼1–3 mm yr^{-1} (Hustand *et al.* 2003; D'Agostino *et al.* 2008; Devoti *et al.* 2011; Riguzzi *et al.* 2013; Carafa *et al.* 2015).

Compelling evidence from seismicity and historical records (Rovida *et al.* 2011) suggests that the strongest earthquakes in the central Apennines are released by normal faults. In fact, the epicentres of $M > 5$ events since ∼1300 A.D. (Fig. 1) appear clearly related to many of these structures (Valensise & Pantosti 2001). Therefore, earthquakes caused by active normal faults represent a major threat in central Italy, as testified by widespread destruction, huge economic losses, and ∼35 000 casualties occurred in the past 100 yr in this region. This is why the

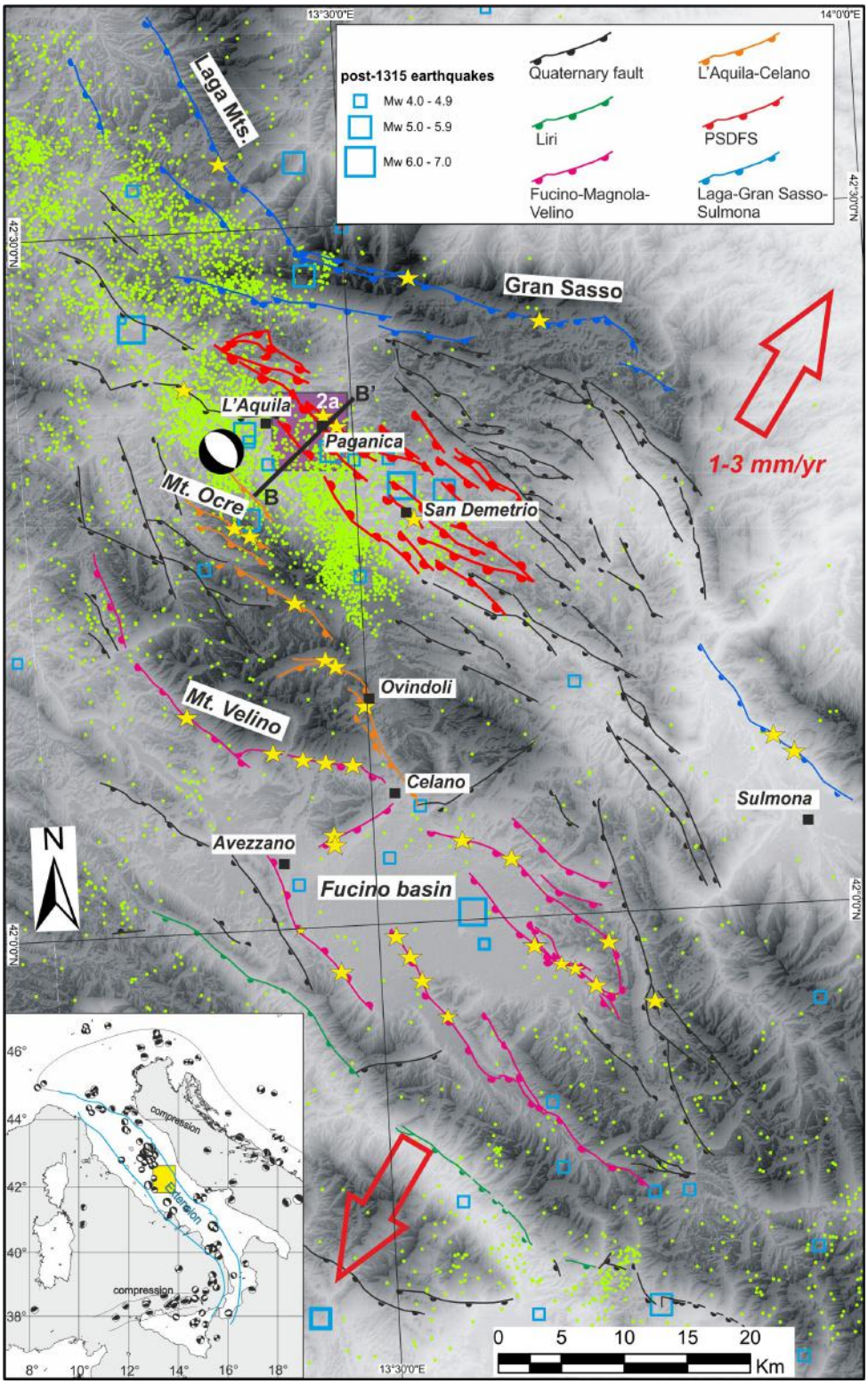

Figure 1. Simplified map of the Quaternary faults and the main active fault-systems in the central Apennines represented with different colour codes (modified after: Villani *et al.* 2015b). In this work, we discuss mainly the Paganica –San Demetrio fault-system (PSDFS), with the Paganica Fault located in the northern part. Green dots indicate $M > 2$ earthquakes in the 1981–2015 period (from the Italian Seismological Instrumental and Parametric Database, ISIDE, http://iside.rm.ingv.it/iside/standard/index.jsp), and the focal mechanism of the 2009 April 6 main shock is shown. Blue squares indicate historical earthquakes (Rovida *et al.* 2011). The yellow stars indicate sites with estimation of Late Pleistocene-Holocene slip-rates on the basis of palaeoseismology or geochemical dating (Galli *et al.* 2008; Benedetti *et al.* 2013; details in the text). Red open arrows show the direction of the current regional extension. The black line B-B′ is the trace of the interpretative section shown in Fig. 11. The purple box encloses the study area (Paganica basin) shown in Fig. 2(a). Inset map: outline of the Italian peninsula with focal mechanisms of $M > 4.5$ earthquakes between 1976 and 2005; the blue lines include the zone of active extension affecting the whole Apennines axis (modified after: Chiarabba *et al.* 2005); the yellow box indicates the area shown in Fig. 1.

characterization and understanding of the fault's seismic behaviour is a critical issue.

The normal faults network dissecting the central Apennines axis consist of 5–10-km-long individual segments, mostly NW-trending and SW-dipping, typically arranged in over-stepping strands and forming systems up to 25–30 km long (Galadini & Galli 2000; Morewood & Roberts 2000; Cowie & Roberts 2001; Roberts *et al.* 2002, 2004). Some of these normal faults may re-utilize older structures, like Mesozoic normal faults and/or Miocene–Pliocene high-angle thrusts (Tavarnelli 1999). In the area shown in Fig. 1, we have grouped the main known active normal fault-systems into five sub-parallel arrays with different colours. Several attempts to estimate their slip-rates and contribution to the regional extension have recently been done: the adopted methods (geodesy, seismic moment summation, palaeoseismology and analysis of long-term offset geological markers) explore the faults behaviour at different timescales (10^1–10^4 yr), and with different spatial resolution (see a discussion in: Faure Walker *et al.* 2010). In particular, palaeoseismic and geochemical data (spanning 10^3–10^4 yr timescale) revealed that strong earthquakes ($6 \leq M \leq 7$) occurred during the Late Pleistocene–Holocene along the following fault-systems: Liri (Roberts 2006); Velino-Magnola and Fucino (Michetti *et al.* 1996; Galadini & Galli 1999; Benedetti *et al.* 2013 and references therein); L'Aquila-Celano (Giraudi 1995; Pantosti *et al.* 1996; Salvi *et al.* 2003); Paganica–San Demetrio (PSDFS; see Section 2) and adjacent faults (Moro *et al.* 2002, 2013; Cinti *et al.* 2011; Blumetti *et al.* 2015); Laga Mts and Gran Sasso (Galli *et al.* 2002; Galadini & Galli 2003); Sulmona and adjacent faults (Falcucci *et al.* 2011; Gori *et al.* 2011; Galli *et al.* 2015). For these faults, individual Late Pleistocene–Holocene slip-rates are estimated in the 0.2–1.3 mm yr^{-1} range, and in most cases they are <0.5 mm yr^{-1}. Furthermore, Faure Walker *et al.* (2010) refined and expanded previous regional analyses of normal fault slip to 10^4 yr timescales (Roberts 2006) by integrating geodetic, palaeoseismic and geomorphic data: their resulting estimate of the averaged extension-rates across the axial zone of the central Apennines in the last 1.2–1.8×10^4 yr is 1.0 ± 0.1 mm yr^{-1}.

Although a conspicuous amount of data concerning the short-term slip-history of a significant number of these normal faults is now available, many of them still lack a complete characterization in terms of shallow structure, geometry, and long- to middle-term slip-rates, which are basic ingredients for a thorough seismic hazard assessment. This lack of information is mainly due to the limited number of high-resolution multidisciplinary studies of the widespread Quaternary hangingwall basins created by long-term normal faulting (Cavinato & De Celles 1999; Ghisetti & Vezzani 1999; Bosi *et al.* 2003). Indeed, the knowledge of the intermediate depth (some tenths to a few hundred metres) basin setting provides key elements for understanding the geometry and slip-rates of the bounding active faults (e.g. amount of Quaternary cumulative displacement; hierarchy of splays, partitioning of deformation and kinematic changes through time within complex fault-systems; see discussion in: Villani *et al.* 2015a,b). Consequently, the scarcity of such studies in the central Apennines hampers a comprehensive imaging of seismogenic faults and a systematic compilation of slip-rates at long timescales (>10^4–10^5 yr).

As a case-study, here we report the example of the fault responsible for the 2009 April 6 M_w 6.1 earthquake, which struck L'Aquila town and surrounding villages causing 309 deaths and widespread destruction (Fig. 1; D'Amico *et al.* 2010; Scognamiglio *et al.* 2010; Herrmann *et al.* 2011). Seismologic data defined the geometry, dimensions and kinematics of the main shock fault, which has been subsequently identified as the Paganica Fault (among others: Chiarabba *et al.* 2009; Chiaraluce 2012; Cirella *et al.* 2012; details in Section 2), and geodetic studies (Atzori *et al.* 2009) indicate that coseismic slip induced maximum subsidence of ~0.25 m in its hangingwall. Active fault geometry and structure at depth in the epicentral area is derived by high-precision relocation of ~64 000 aftershocks of the 2009 earthquake sequence (Chiaraluce *et al.* 2011; Valoroso *et al.* 2013), highlighting a 2 to ~12-km-deep picture of SW-dipping crustal faults and related antithetic splays. To characterize the geometry and structure of the seismically active fault, very shallow geophysical investigations were performed near L'Aquila targeting the intermediate-depth subsurface (Balasco *et al.* 2011; Giocoli *et al.* 2011; Improta *et al.* 2012; Pucci *et al.* 2016), and these pointed out two small tectonic basins (Fig. 2a): the Paganica basin, in the hangingwall of the Paganica Fault, and the Bazzano basin, located to the south of Mt Bazzano (Fig. 2a). Improta *et al.* (2012) propose a simplified geological section across the Bazzano basin and the southernmost part of the Paganica basin using high-resolution (HR) seismic tomography; they also present a first rough estimate of the Paganica Fault total throw (>250 m).

Notwithstanding the massive post-earthquake studies, many questions on the relations between the uppermost and the deep crustal structural settings are still open. The establishment of this connection is even more difficult due to the lack of commercial reflection profiles for the L'Aquila region, which exist only for areas several km to the north and to the south (Cavinato *et al.* 2002; Patacca *et al.* 2008; Bigi *et al.* 2011).

In order to improve our understanding of these relations, we applied HR refraction tomography with two dense, wide-aperture profiles acquired across the Paganica Fault. We follow an approach based on the integration of seismic imaging with detailed geological and fault mapping in order to get a reliable 2-D subsurface model of a very complex fault-bounded setting. Our primary targets are: (1) HR shallow imaging of the Paganica Fault and detection possible buried splays; (2) reconstruction of the hangingwall basin geometry; (3) estimation of the long-term displacement accrued by the investigated fault-system and (4) connection between the surface structural features and the deep seismogenic source.

By combining the tomographic images from the two seismic profiles, and complementing them with detailed geological data, we propose a shallow (~2 km deep) semi-quantitative structural model of the Paganica basin. This represents a thoroughly updated subsurface image with respect to some previously published simplified cross-sections (see for instance: Balasco *et al.* 2011; Improta *et al.* 2012; Lavecchia *et al.* 2012). We use this model to assess the long-term slip history of the Paganica Fault and to explore the possible link between the surface and the earthquake fault at depth by taking advantage of the available huge amount of the 2009 relocated aftershocks. The integration of these different types of data belonging to very shallow, intermediate-depth and deep structural levels in the upper crust represents a quite unique opportunity in the whole Mediterranean area to investigate the anatomy and long-term evolution of a major seismogenic fault.

2 GEOLOGICAL BACKGROUND

2.1 The Paganica Fault: summary of existing geological data

The Paganica Fault is the northwestern portion of the Paganica–San Demetrio fault-system (hereinafter referred as PSDFS; Galli *et al.* 2010; Civico *et al.* 2015), which is a ~19–20-km-long system of

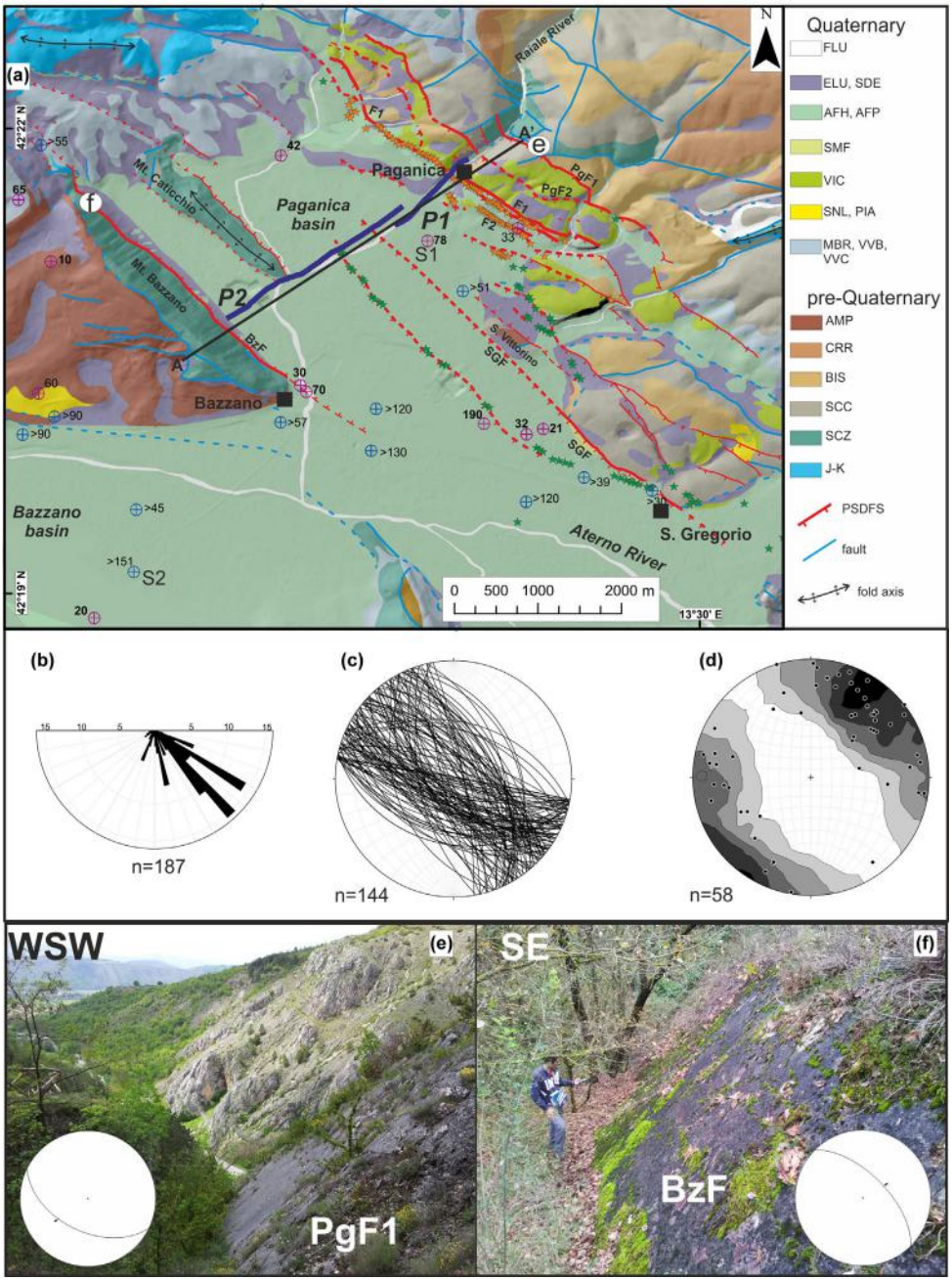

Figure 2. (a) Geological sketch of the Paganica and Bazzano basins (modified after: Centamore *et al.* 2006; Pucci *et al.* 2015): FLU: fluvial deposits (Holocene); ELU, SDE: colluvium and slope debris (Late Pleistocene–Holocene); AFH-AFP: alluvial gravels and sands (Late Pleistocene–Holocene); SMF: fluvial gravels and sands (San Mauro *Fm.*, Middle Pleistocene); VIC: fluvial and alluvial conglomerates (Valle Inferno *Fm.*, Early Pleistocene); SNL-PIA: lacustrine silts (San Nicandro and Pianola *Fms.*, Early Pleistocene); MBR, VVB, VVC: breccia and conglomerates (Megrabrecce and Valle Valiano *Fms.*, Early Pleistocene); AMP: flysch (Late Miocene); CRR: Cerrogna *Fm.* (Middle-Late Miocene); BIS: Bisciaro *Fm.* (Early Miocene); SCC: Scaglia Cinerea *Fm.* (Eocene–Early Miocene); SCZ: Scaglia Detritica *Fm.* (Cretaceous - Eocene); J–K: undifferentiated Late Jurassic–Early Cretaceous formations (Calcari a Fucoidi *Fm.*, CFF; Maiolica Detritica *Fm.*, MAD; Calcari Diasprigni Detritici *Fm.*, CDI; Verde Ammonitico *Fm.*, VAP; Corniola *Fm.*, COI). The red lines indicate the main traces of the PSDFS (dashed where blind and/or inferred). The thin blue lines are normal faults. SGF, F1, F2, BzF, PgF1 and PgF2 are faults discussed in Sections 2, 5 and 6. The orange and green stars are sites of coseismic surface breaks observed, respectively by Emergeo Working Group (2010) and Boncio *et al.* (2010). The open circles with cross represent shallow boreholes reaching (pink) and not reaching (blue) the pre-Quaternary basement, respectively (numbers indicate basement depth in metres). The bold dark blue lines are the seismic profiles P1 and P2. The black line A–A′ indicates the geological cross-section shown in Fig. 10. Location of structural sites in panels (e) and (f) is shown with white circles. (b) Rose diagram indicating the trend of 187 fault segments included in the area reported in panel (a) (total length: 100.6 km; the modal direction class is N135°–140°). (c) Equal area projection of 144 selected fault planes affecting basement rocks in the study area. (d) Contour plot of poles to planes of 58 fault affecting Quaternary deposits in the study area (contour interval: 1 per cent). (e) Panoramic view to the WSW from the main splay of fault PgF1: fault attitude (dip-direction/dip-angle notation) 206°/50°, pitch 70°SW; inset stereoplot with kinematics; site location in panel (a). (f) Close-up view of the northern portion of fault BzF: fault attitude: 45°/65°, pitch 80°NE; inset stereoplot with kinematics; site location in panel (a).

normal faults bounding to the east the wide Quaternary continental basin of the Middle Aterno Valley (Figs 1 and 2a; Bosi *et al.* 2003). As reported by different authors (Bagnaia *et al.* 1992; Bertini & Bosi 1993), and according to recent geological mapping (Pucci *et al.* 2015), the Middle Aterno Valley area is affected by a limited amount of shortening, which is mostly confined to the north (Gran Sasso sector; Ghisetti & Vezzani 1991; D'Agostino *et al.* 1998) and to the south (Mt Ocre sector: Vezzani & Ghisetti 1998; Centamore *et al.* 2006). A few studies focusing on the geological and geomorphological setting of the Middle Aterno Valley (Galli *et al.* 2010; Giaccio *et al.* 2012; Blumetti *et al.* 2013, 2015; Civico *et al.* 2015; Pucci *et al.* 2015; Villani *et al.* 2015b) support the evidence that the PSDFS is an active structure composed of several and mostly SW-dipping splays that displace Mezo-Cenozoic marine carbonate rocks and the overlying Quaternary continental sequence with hundreds of metres of morphologic throw, thus originating a basin-and-range landscape.

Before the 2009 L'Aquila earthquake, the Paganica Fault was not fully mapped (Bagnaia *et al.* 1992; Vezzani & Ghisetti 1998; Centamore *et al.* 2006) and its seismogenic potential was assessed only by a few authors (Boncio *et al.* 2004; Pace *et al.* 2006; Akinci *et al.* 2009). During the 6 April main shock, this fault created a coseismic surface displacement clearly observed for a total length >3 km (Fig. 2a), and consisting of a complex set of small scarps (up to 0.10–0.15 m high) and open cracks (Falcucci *et al.* 2009; Emergeo Working Group 2010; Vittori *et al.* 2011). After the earthquake, a wealth of geological investigations were carried out to understand the possible link of the surface ruptures with the seismogenic structures (Boncio *et al.* 2010; Galli *et al.* 2010; Roberts *et al.* 2010; Lavecchia *et al.* 2012), and the pre-historic behaviour of the fault through palaeoseismic trenching (Cinti *et al.* 2011; Galli *et al.* 2011; Moro *et al.* 2013). These new studies revealed that the Paganica Fault is responsible for episodic large earthquakes ($M \sim 6$ or greater), as highlighted by palaeoseismic data and by the historical record of seismicity in the area (Tertulliani *et al.* 2009; Rovida *et al.* 2011). According to Cinti *et al.* (2011), this fault accommodates 0.25–0.33 mm yr^{-1} post-30 ka throw-rate, accounting for dip-slip rates of ~0.3–0.4 mm yr^{-1}. Galli *et al.* (2010), by studying offset of Middle and Late Pleistocene fluvial terraces and deposits, suggest a slip-rate of ~0.5 mm yr^{-1} in the last 0.5 Myr. Civico *et al.* (2015), based on the cumulative offset of several geomorphic markers accrued during the Quaternary, report ~250–300 m of total morphologic throw for the Paganica Fault along a cross-section parallel to the seismic profiles discussed in this paper.

Basically, the aforementioned works interpret the small 2009 primary ruptures and the palaeoseismic record of past surface faulting events as due to the upward propagation of coseismic slip at depth: therefore, the Paganica Fault is considered as a crustal normal fault, even though aftershocks alignment illuminate this structure only in the ~2–10 km depth range (Chiaraluce *et al.* 2011; Valoroso *et al.* 2013), and geodetic modelling suggests that the 2009 seismic dislocation (peak value of ~0.9 m) stopped at ~1 km depth (Atzori *et al.* 2009). However, there is still debate on the connection between the Paganica Fault at the surface and the deep seismogenic source. For instance, Bonini *et al.* (2014) propose a radically different interpretation, mostly based on the outcomes of analogue modelling: they infer that the 2009 seismogenic fault is confined between ~3 and 10 km depth, and that slip observed at the surface after the earthquake represents pseudo-primary breaks caused by crustal bending and sympathetic slip on shallow secondary faults. Speranza & Minelli (2014), from magnetic and gravimetric modelling of the 2009 earthquake area, point out an anomalous thickness of Triassic–Early Jurassic dolomites to the south of L'Aquila in the ~3–12 km depth range, and they propose an evolutionary model where the Paganica Fault re-activates during the Quaternary an early Mesozoic normal fault previously responsible for the dolomites thickening, and which was inverted during Miocene–Pliocene compression as a high-angle thrust.

2.2 The Paganica basin: revised and new geological data

To increase the amount of information useful to constrain the geological interpretation of our seismic profiles, we collected additional structural and stratigraphic data regarding both Quaternary continental formations and marine Mesozoic–Cenozoic rocks (that we call for simplicity basement), outcropping in the Paganica basin. In particular, we have concentrated our attention on the characteristics and age of the stratigraphic units we were potentially imaging at depth in the seismic sections, and on the geometry and kinematics of the tectonic structures (faults) that could dissect the basin filling sediments. Recently published data (Boncio *et al.* 2010; Giaccio *et al.* 2012; Lavecchia *et al.* 2012; Pucci *et al.* 2015) were used as main reference. The most significant results of our structural analysis are summarized in Figs 2(b)–(d). We checked thickness of formations in the field and collected >440 bedding plane attitude measurements. We also checked for a limited number of shallow boreholes reaching the basement (Fig. 2a), providing only a few constraints on the subsurface geometry of the Paganica basin.

As regards the stratigraphic setting, basement rocks consist of a Cretaceous-Miocene marly-carbonatic marine sequence: Scaglia Detritica *Fm.* (SCZ, ~200 m thick); Scaglia Cinerea *Fm.* (SCC, ~250–350 m thick); Bisciaro *Fm.* (BIS, ~150 m thick), covered by Late Miocene calcareous–arenaceous flysch (AMP, ~90–100 m thick in the central part, >200 m thick in the eastern part of the basin). At the northern edge of the area, and along the upper reaches of the Raiale River gorge, Early Jurassic–Cretaceous marly limestones and cherts crop out (unit J–K in Fig. 2a; further details in Fig. 10). The Quaternary sequence overlies unconformably the basement and is composed of loose to well-cemented alluvial fan, fluvial and lacustrine sediments with widespread depositional hiatuses. These sediments exhibit variable thickness (between 20 and >100 m) and complex heteropic relationships (Pucci *et al.* 2015). From the bottom to the top, the main formations are (Fig. 2a): chaotic breccia and alluvial fan conglomerates (units MBR, VVC and VVB); lacustrine silts and sands (units PIA and SNL); alluvial conglomerates (unit VIC); fluvial and alluvial conglomerates and sands (units SMF, AFP and AFH).

We carried out field surveys to assess the local structural setting and accurately map the strands of the PSDFS with evidence of Quaternary activity (marked in red in Fig. 2a). Along the NE border of the Paganica basin, basically two main sets of active faults are recognized, displaying a right-stepping relationship, a separation of ~1 km and an overlap >1.5 km: (1) the first one, near Paganica, consists of four main closely spaced and SW-dipping splays (PgF1, PgF2, F1 and F2 in Fig. 2a) with an overall length of ~5.8 km; (2) the second one, consists of a main SW-dipping strand with an overall length of ~4.8 km (SGF in Fig. 2a) and subordinate splays in the footwall. The SW part of the Paganica basin is bounded by the 4.7-km-long and NE-dipping Bazzano Fault (BzF in Fig. 2a). The complex pattern of Quaternary deformation is further testified by

Table 1. Main characteristics of the seismic profiles.

Profile name	Length	Receiver spacing	Average shot spacing	Picked CSG	Maximum offset	Picked traces	Rms picking uncertainty
P1	1075 m	5 m	10 m	107	437.5 m	9695	2.2 ms
P2	2095 m	5 m	10 m	164	775 m	23 950	2.6 ms

the occurrence of several other minor splays, with lengths of a few hundred metres, and some small intrabasin basement horsts (e.g. Mt Caticchio, S. Vittorino in Fig. 2a). The primary coseismic surface breaks were observed mostly along faults F1 and F2 (orange stars in Fig. 2a).

We performed a directional analysis of the mapped faults using a GIS tool that simplifies fault traces, and then calculates the average strike of each segment. The obtained values are weighted according to segment length, and the resulting rose diagram is shown in Fig. 2(b). This plot indicates that the overall fault pattern is dominated by NW-trending segments, up to 3 km long (modal class N135°–140°, followed by N120°–125°). This analysis further shows that subordinate structures trending N165°–170° and N110°–115° are also present.

We collected >460 measurements of fault plane attitude on both Quaternary and basement rocks. Fig. 2(c) shows a selection of measurements from the faults belonging to the dominant directional classes: this analysis points out a different average dip of the SW-dipping and NE-dipping splays, being ∼58° ± 15° and ∼70° ± 15°, respectively. Fig. 2(c) shows a contour density plot of poles to fault planes affecting Early to Late Pleistocene deposits, still indicating the persistent Quaternary activity of the NW-striking segments of the PSDFS.

The poor preservation of kinematic indicators on fault planes affecting basement rocks hampers a thorough analysis. However, in some sites we were able to document a nearly pure dip-slip normal kinematics of the NW-trending faults (pitch values generally >70°; Figs 2e and f).

Absolute dating of continental deposits older than ∼0.6 Myr is lacking in the study area (unit SMF in Fig. 2a; Galli *et al.* 2010), and this does not allow an accurate timing of the older tectonic and stratigraphic events. We recognized in the Paganica basin the presence of Early Pleistocene lacustrine deposits (SNL *Fm.*) and alluvial fan conglomerates (VIC *Fm.*). Correlations with the adjacent San Demetrio sector, and palaeomagnetic investigations demonstrate that the upper part of the SNL *Fm.*, together with some heteropic continental breccia, are ∼1.3 Myr old (Giaccio *et al.* 2012 and references therein). Mancini *et al.* (2012) relate to the Gelasian (lower part of Early Pleistocene, 1.80–2.59 Ma) the basal conglomerates of the continental succession to the west of L'Aquila, very close to Paganica. Similarly, new biostratigraphic data from the basal part of the SNL *Fm.* (Spadi *et al.* 2015) suggest a Gelasian age for the beginning of the lacustrine sedimentation in the San Demetrio sector. Stratigraphic data from a 150-m-deep borehole in the Bazzano basin (S2 in Fig. 2a; Macrì *et al.* 2016; Porreca *et al.* 2016) suggest that the fluvial silts and sands layers recovered at a depth >115 m are Early Pleistocene in age.

Furthermore, plenty of evidence from the nearby Fucino basin and other adjacent continental depressions (Cavinato *et al.* 2002; Bosi *et al.* 2003; Roberts *et al.* 2004; Whittaker *et al.* 2010) support an inception age of the extensional tectonics in this sector of the chain axis between 2 and 3 Ma. For all these reasons, it is highly probable that continental deposition in the Paganica basin took place during the Gelasian, which gives the minimum age of local post-orogenic extensional tectonics.

3 SEISMIC DATA AND NON-LINEAR TOMOGRAPHIC INVERSION

The seismic dataset used in this paper consists of two HR seismic profiles (P1 and P2 in Fig. 2a) acquired in 2010: they run SW-NE for a total length ∼3 km across the Paganica basin and intersect the 2009 primary coseismic ruptures. The two profiles are spaced ∼100 m apart and overlap for 230 m. Profile P1 and the northern part of profile P2 were acquired in the Paganica village, and thus required great efforts to collect good quality data. Improta *et al.* (2012) already used a limited subset of data from profile P2. In this paper, we report for the first time results from profile P1 that crosses the Paganica Fault, and we also show new results for profile P2 obtained by a new tomographic inversion of a larger amount of data.

The acquisition layout consisted of a 216 channels and 1075-m-long array deployed with 5 m spacing between the 10-Hz vertical sensors. We adapted the dense wide-aperture acquisition strategy used in hydrocarbon exploration of complex structures (Operto *et al.* 2004; Ravaut *et al.* 2004) to shallow targets, aimed at collecting highly redundant P-pulses corresponding to shallow direct waves and deep-penetrating turning waves and critical refractions, suitable for multiscale traveltime tomography (Bruno *et al.* 2013). The wide aperture of the recording array was ∼10 times larger than the presumed bedrock depth near the Paganica Fault (∼100 m) and ∼3 times larger than the maximum depth to basement within the Paganica basin (∼300 m). We acquired profile P1 with a fixed array, whereas for profile P2 the array was moved with a roll-along technique to attain 2095 m length. As seismic source we used a single 6400 kg IVI-MINIVIB® vibroseis truck. For each vibration-point we recorded the stack of three, 15 s long, 5–200 Hz linear upsweeps, and source move-up was 5–10 m (Table 1). Seismic data were recorded using nine 24-bit seismographs, and setting a sampling rate of 1.25×10^{-4} s.

HR refraction tomography has widely been recognized as a powerful tool to image complex media such as fault structures and tectonic basins filled with heterogeneous sediments (Morey & Schuster 1999; Calvert & Fisher 2001; Improta *et al.* 2003; Sheley *et al.* 2003; Mattson 2004; Pelton 2005; Catchings *et al.* 2008; Bruno *et al.* 2013; Dìaz *et al.* 2014). In such complex environments, conventional seismic reflection imaging by common-mid-point profiling is usually hampered by near-surface heterogeneities, strong diffractions associated to coarse clastic infill, sharp lateral velocity variations, which are adequately handled by seismic tomography (Improta *et al.* 2010).

In this work, we used a non-linear multiscale tomography (Improta *et al.* 2002) that does not require a starting reference model and is able to cope with very heterogeneous media (Improta *et al.* 2003; Improta & Corciulo 2006; Improta & Bruno 2007; Bruno *et al.* 2010a,b, 2013; Villani *et al.* 2015a,b). The input data consist of >30 000 first arrival traveltimes, which we hand-picked on raw or bandpass-filtered traces of 107 (profile P1) and 164 (profile P2) selected common shot gathers (CSG, details in Table 1). The picking strategy is based on the reading of a time window (t1, t2) bracketing the presumed traveltime. The cost function used in the tomographic inversion is a least-squares L^2 norm, defined as

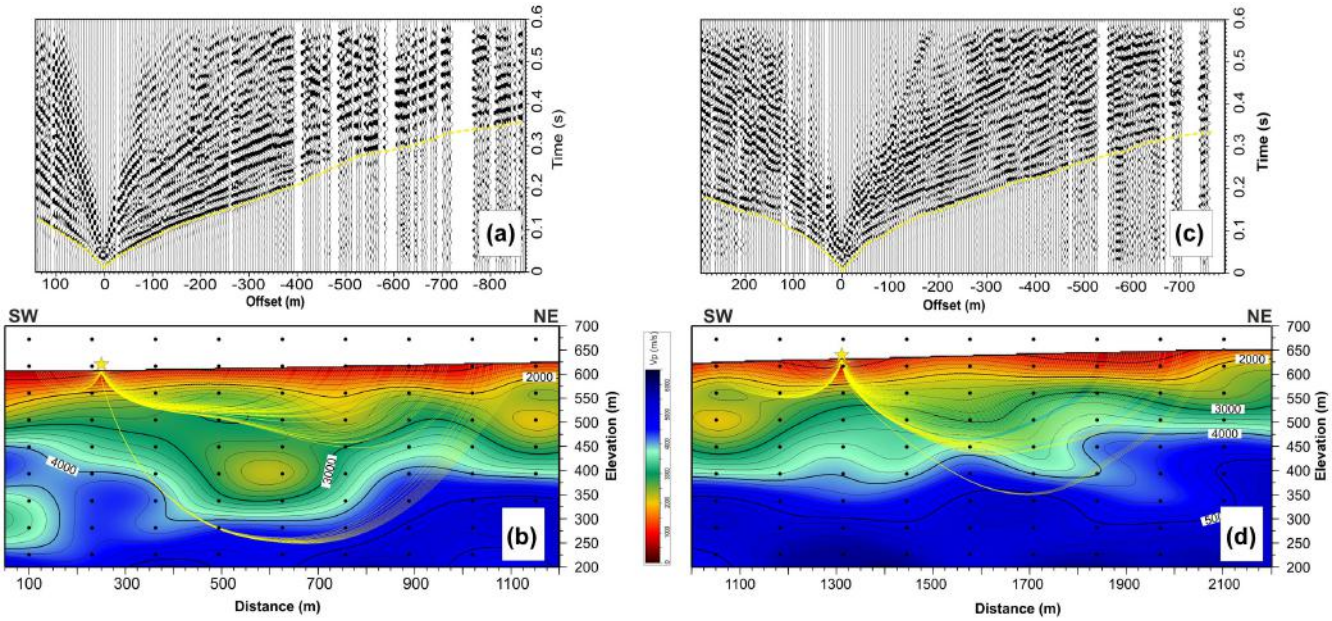

Figure 3. (a) Profile P2, CSG 191 with picking of first breaks (yellow dashed line); (b) back-ray tracing for CSG 191 superimposed on the long-wavelength tomographic model; (c) profile P2, CSG 74 with picking of first breaks (yellow dashed line) and (d) back-ray tracing for CSG 74 superimposed on the long-wavelength tomographic model.

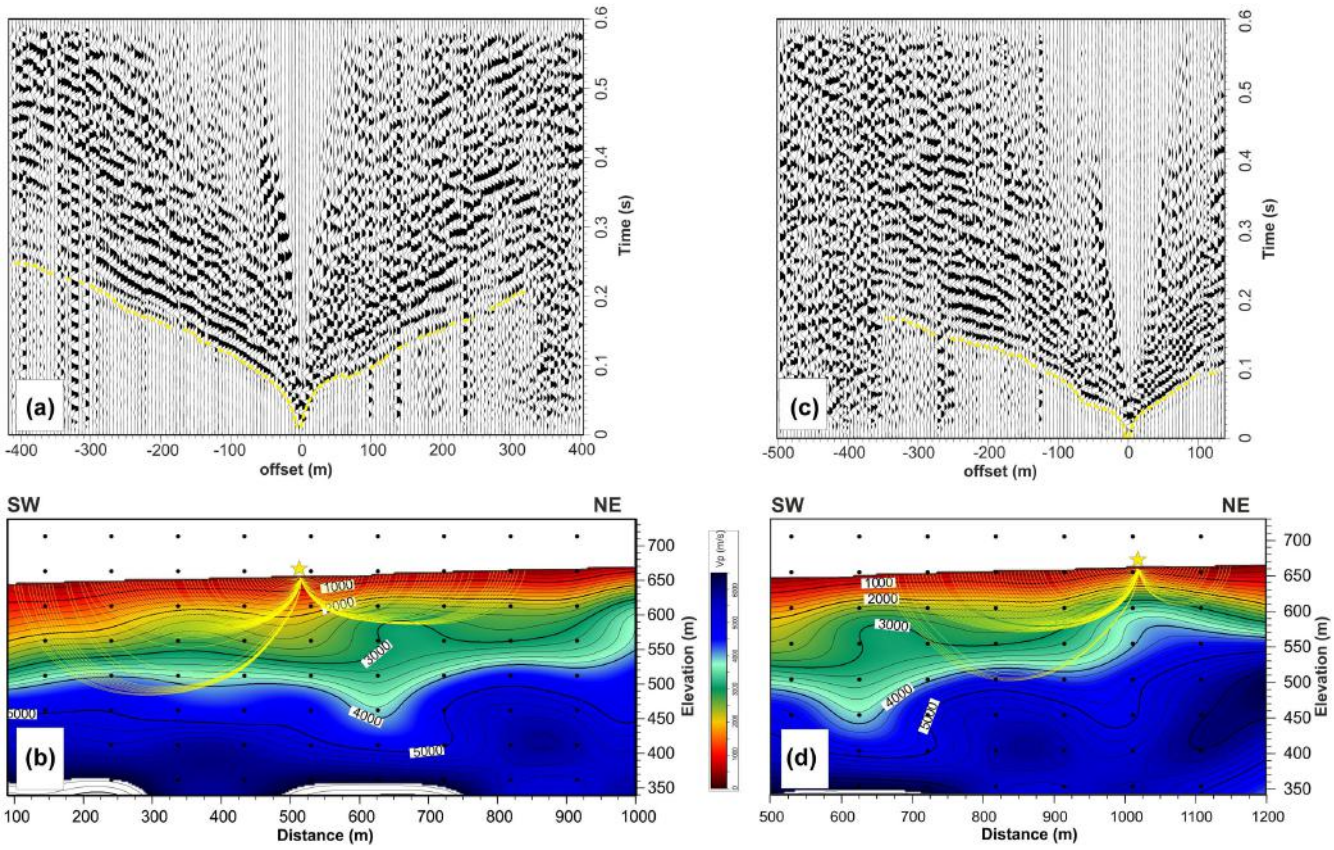

Figure 4. (a) Profile P1, CSG 40 with picking of first breaks (yellow dashed line); (b) back-ray tracing for CSG 40 superimposed on the long-wavelength tomographic model; (c) profile P2, CSG 110 with picking of first breaks (yellow dashed line) and (d) back-ray tracing for CSG 110 superimposed on the long-wavelength tomographic model.

the sum of the weighted squared differences between observed and computed traveltimes, and data weighting is related to the inverse t1–t2 time window. The seismic sections show moveout of first breaks suggesting the presence of severe velocity heterogeneities and deep high-*Vp* refractors (Figs 3 and 4). Due to the highly variable quality of the dataset, the maximum offset of readable first breaks was ∼430 m for profile P1 and ∼770 m for profile P2. The peak frequency of the first arrival wavelet is generally centred at

50–70 Hz, which implies a first Fresnel zone radius (Williamson & Worthington 1993) <60 m in the near offset (<100 m) considering an average $Vp \sim 2000$ m s^{-1} for the shallow layers (<100 m depth).

In this tomographic inversion procedure, first-arrival traveltimes are computed by a finite-difference Eikonal solver accounting for transmitted, diffracted and head waves (Podvin & Lecomte 1991). Based on the acquisition geometry and receiver spacing, we set a fixed and dense 2.5-m finite-difference mesh that allows computing very accurate traveltimes. *P*-wave velocity values at each node of the finite-difference mesh are assigned by a b-cubic spline interpolation between velocity nodes of a coarse grid. These latter are the parameters of the tomographic inversion. The multiscale strategy consists in a succession of inversion runs performed by gradually reducing the spacing of the velocity nodes (i.e. progressively increasing the number of model parameters). At each inversion run, a non-linear algorithm combining global random search (Monte Carlo) with local search (Simplex) finds the best-fitting model. The best-fit model is then used as reference in a subsequent inversion run that is performed with a larger number of parameters. The models obtained at the early inversion runs (*long-wavelength* models or *macro-models*) define the large-scale structure of the medium, while the models with a higher number of parameters obtained at the subsequent inversion runs (*short-wavelength* models) illuminate the near-surface with an increased spatial resolution (Lutter & Nowack 1990). However, the increase in the spatial resolution implicit in multiscale inversion strategy is achieved at the cost of a progressive decrease in resolution depth. *A posteriori* checkerboard tests (Hearn & Ni 1994) are used to estimate the model resolution and the ability of the non-linear tomographic inversion to resolve subsurface structural details. For each best-fit velocity model, we performed checkerboard tests by applying to the 2.5 m finite-difference mesh a smooth 2-D Gaussian perturbation pattern (velocity range ±50 or ±100 m s^{-1}) with maxima centred on the bi-cubic spline grid nodes and tapering to zero at half distance between adjacent nodes. The average resolution length is estimated to be approximately equal to half of the recovered checker dimension (Lebedev & Nolet 2003; see a review in: An 2012). Checkerboard tests indicate that in our short-wavelength models bodies whose radius is ∼15 m are resolved. The multiscale inversion procedure is halted based on results of the resolution tests and on the analysis of rms of traveltime residuals run after run.

For each seismic profile, we describe a representative long-wavelength model (grid nodes spacing along X direction ∼120 m) that defines the large-scale structure of the Paganica basin. For profile P1, we also show a short-wavelength model with a higher spatial resolution (grid nodes spacing along *x*-direction ∼35 m), which targets the subsurface of the 2009 primary coseismic ruptures. Below each model, we show the results of a checkerboard test. As additional information, we also include ray-density plots in order to roughly visualize the sampled regions of the tomograms. However, it is worthy to note that the non-linear inversion adopted is not based on ray tracing: ray paths are calculated *a posteriori* with a back-ray tracing procedure (full details in: Podvin & Lecomte 1991), and they are not meant to be used for resolution assessment.

As expected, near-vertical reflections exhibit an overall low quality due to unfavourable local geological conditions and to the presence of severe lateral velocity heterogeneities along the investigated sections. As discussed in Section 5.1, we cross-checked the consistency of tomographic results and the interpretation of the top-basement surface by analysing small-offset deep reflections recognized on several common-mid-point (CMP) gathers. Notwithstanding the 1-D limitation implicit in such kind of analysis, we indeed were able to test whether the top-basement inferred from refraction tomography also corresponds to an important reflecting interface.

4 RESULTS: REFRACTION TOMOGRAPHY ACROSS THE PAGANICA FAULT

Fig. 5(a) shows a representative long-wavelength model of profile P2 with a low number of nodes, and resolved down to ∼250–300 m depth.

Fig. 6(a) shows a long-wavelength model obtained at a later stage of the multiscale inversion with a higher number of nodes, and characterized by a resolution depth of ∼200 m below the surface.

We then integrate the deeper information provided by model in Fig. 5(a) with the higher-resolution surface details of model in Fig. 6(a) for the final structural interpretation (Section 5).

With the exception of a ∼50-m-thick shallower layer with $Vp < 2000$ m s^{-1}, the lower part of the tomogram in Fig. 6(a) shows evident lateral velocity variations approximately at $x = 300$, 600, 950, 1200, 1400 and 1700 m. Here, regions with low vertical gradient and relatively low velocity ($Vp \sim 2400$–3000 m s^{-1}) overlay a deeper high-velocity region ($Vp > 3800$–4000 m s^{-1}) characterized by complex geometry with considerable depth variations (locally >150 m).

Fig. 7(a) shows a representative long-wavelength model of profile P1 characterized by a resolution depth of ∼150–180 m below the surface.

Strong lateral *Vp* changes are indicative of high-angle discontinuities located approximately at $x = 450$, 550 and 800–850 m, whereas low-*Vp* regions (1400–2400 m s^{-1}) thicken above their down-dipping side. The short-wavelength tomogram of profile P1 (Fig. 8a) was obtained at a later stage of the multiscale inversion by cutting the model shown in Fig. 7(a), and using a node spacing of 35 m along the *x*-direction and 25 m along the *z*-direction.

Checkerboard test indicates that the model is well resolved down to ∼100–120 m depth: the average radius of the recovered checker in this case is ∼15 m, which enables depicting confidently the very shallow subsurface setting with a fine spatial resolution The same discontinuities inferred by the long-wavelength model (Fig. 7a) are further detailed in this new model at $x = 50$–150 m and at $x = 450$–500 m, and they can be traced up to a few metres depth from the ground surface. Notably, a thickening (>20 m) of the near-surface very low-*Vp* layer (<1000 m s^{-1}) is evident at $x = 300$–450 m.

5 INTERPRETATION OF THE *Vp* TOMOGRAMS

5.1 The pre-Quaternary basement beneath the continental cover

The geo-structural interpretation of the tomograms is reported in Fig. 9, whereas in Fig. 10 we show the geological section across the Paganica basin resulting from the merge of *Vp* images of seismic profiles P1 and P2 integrated with geological data.

A key element in this interpretation is the boundary between the continental basin infill and the pre-Quaternary basement (white dashed line in Fig. 9). We interpret this boundary to be located in a high-gradient (∼20 m thick) zone of the tomograms, where *Vp* rapidly increases from 3600 to >4000 m s^{-1}, and ray-density plots (Figs 7c and 8c) suggest a main seismic interface. Fig. S1 shows head-waves generated by this interface as low-amplitude

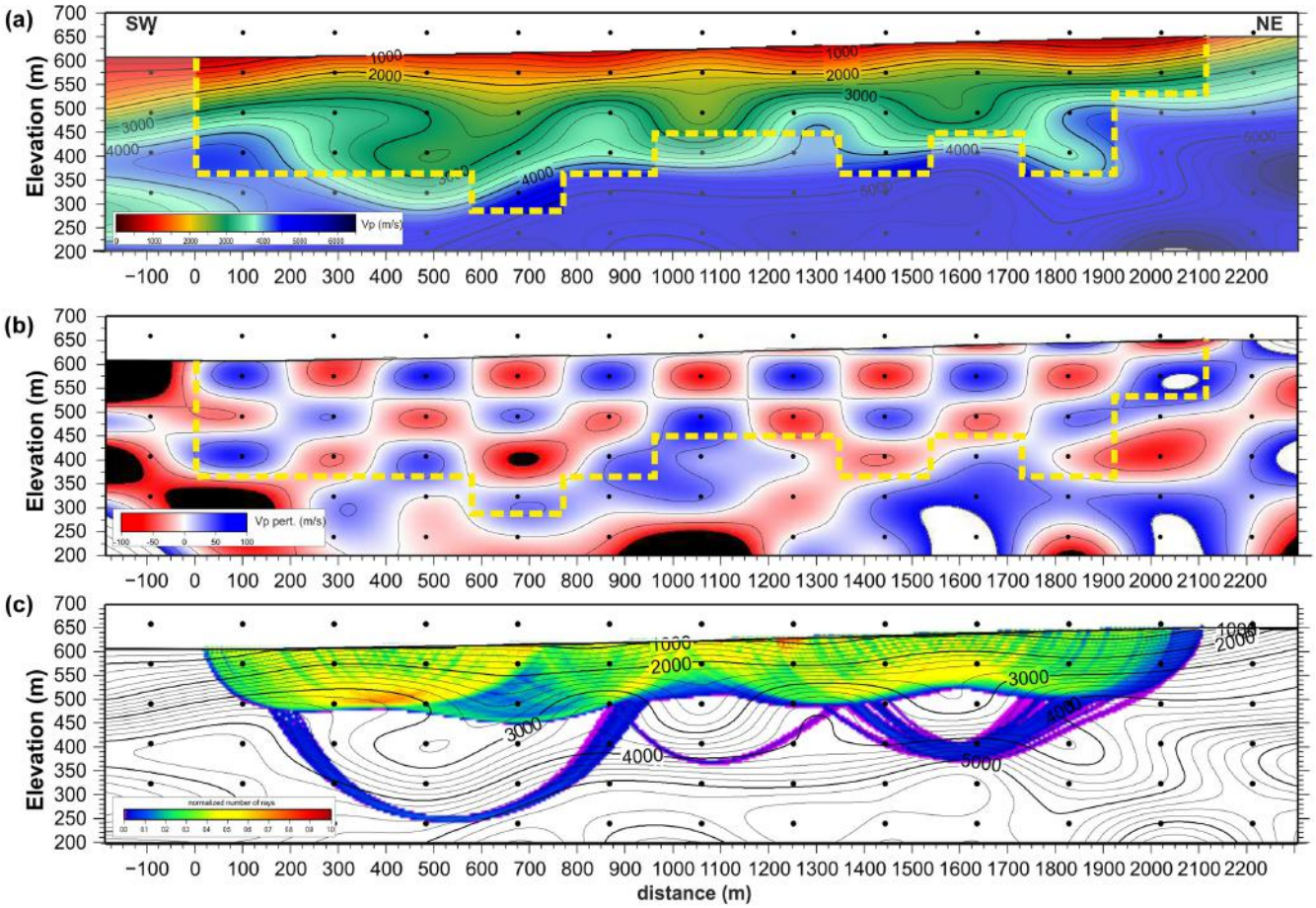

Figure 5. (a) Long-wavelength (78 parameters) *Vp* tomogram of profile P2; the dashed yellow line indicates resolution depth obtained by outlining the lowermost resolved checkers within the grid of velocity nodes; (b) result of checkerboard test and (c) ray-density plot (normalized inside 5 m × 5 m cells).

first arrivals with an apparent velocity >4000 m s^{-1}. Also the inspection of several CMP gathers seems to confirm the nature and location of this interface. In fact, despite the overall low quality and the 1-D limitations of the CMP analysis, these gathers show some large-amplitude reflections from the top-basement with a subtle hyperbolic character, and which can be followed from the large to the small offset range (Figs S2 and S3 in the auxiliary material). Moreover, their high amplitude at large offsets indicates they are wide-angle hypercritical reflections generated by a deep interface with a strong, positive impedance contrast. In order to qualitatively test the consistence between tomographic results and the location of this reflecting interface, we depth-converted 'zero offset' reflected arrivals (t_0) using the average tomographic *Vp* in correspondence of each selected CMP gather: the resulting reflection points fall within the 3600–4000 m s^{-1} high-gradient zone of the tomograms (Fig. 9), confirming that it is the smeared tomographic image of the top-basement.

Additional constraints are given by new field data (Section 2.2), by mapped outcrops (Pucci *et al.* 2015) and by available boreholes (MS-AQ Working Group 2010; Giocoli *et al.* 2011; Fig. 2a). The resolved SW part of the seismic section is tied to outcrops of thick-bedded limestones of the Cretaceous-Eocene SCZ *Fm.*, and the NE part to marly limestones of the Miocene BIS *Fm.* (Fig. 10). Borehole S1 (Fig. 2a), located 320 m to the SE of profile P1, encounters at 78 m depth fractured limestones: we relate these limestones to the top of the BIS *Fm.*, because borehole S1 is in the hangingwall of the Paganica Fault, exposing SW-dipping beds of the BIS *Fm.* in the footwall. Limestones retrieved in this borehole are shallower than the top-basement as imaged on profile P1, indicating a local NW-dip of the basin bottom: this is also suggested by the NW-sloping SCC *Fm.* outcropping to the SE (S. Vittorino, Fig. 2a).

5.2 The continental basin infill

Tomographic data allow us to partition the continental infill in two parts, Q1 and Q2 in Fig. 10, also based on previous seismic investigations in the same area (Improta *et al.* 2012). We interpret low-*Vp* (<2400 m s^{-1}) regions (unit Q2) as shallow fluvial and alluvial fan gravels with sand layers (comprising the AFH, AFP, and SMA *Fms.* in Fig. 2a), by correlating them to quarry outcrops to the east of Mt Bazzano and some boreholes between the Paganica and Bazzano villages (Fig. 2a). We then interpret intermediate-*Vp* (2600–3400 m s^{-1}) regions (unit Q1) as cemented breccia and coarse conglomerates (comprising the MBR, VVB, VVC, and VIC *Fms.* in Fig. 2a). As one can see, the infilling deposits show dramatic changes in thickness (from <20 to >270 m), which we interpret as related to the interactions between faulting and depositional processes.

5.3 Subsurface fault zones

Fault recognition on the tomograms of Fig. 9 is based on two main criteria: (1) the bumpy morphology of the inferred top-basement surface (*Vp* 3600–4000 m s^{-1}) and (2) the presence of evident

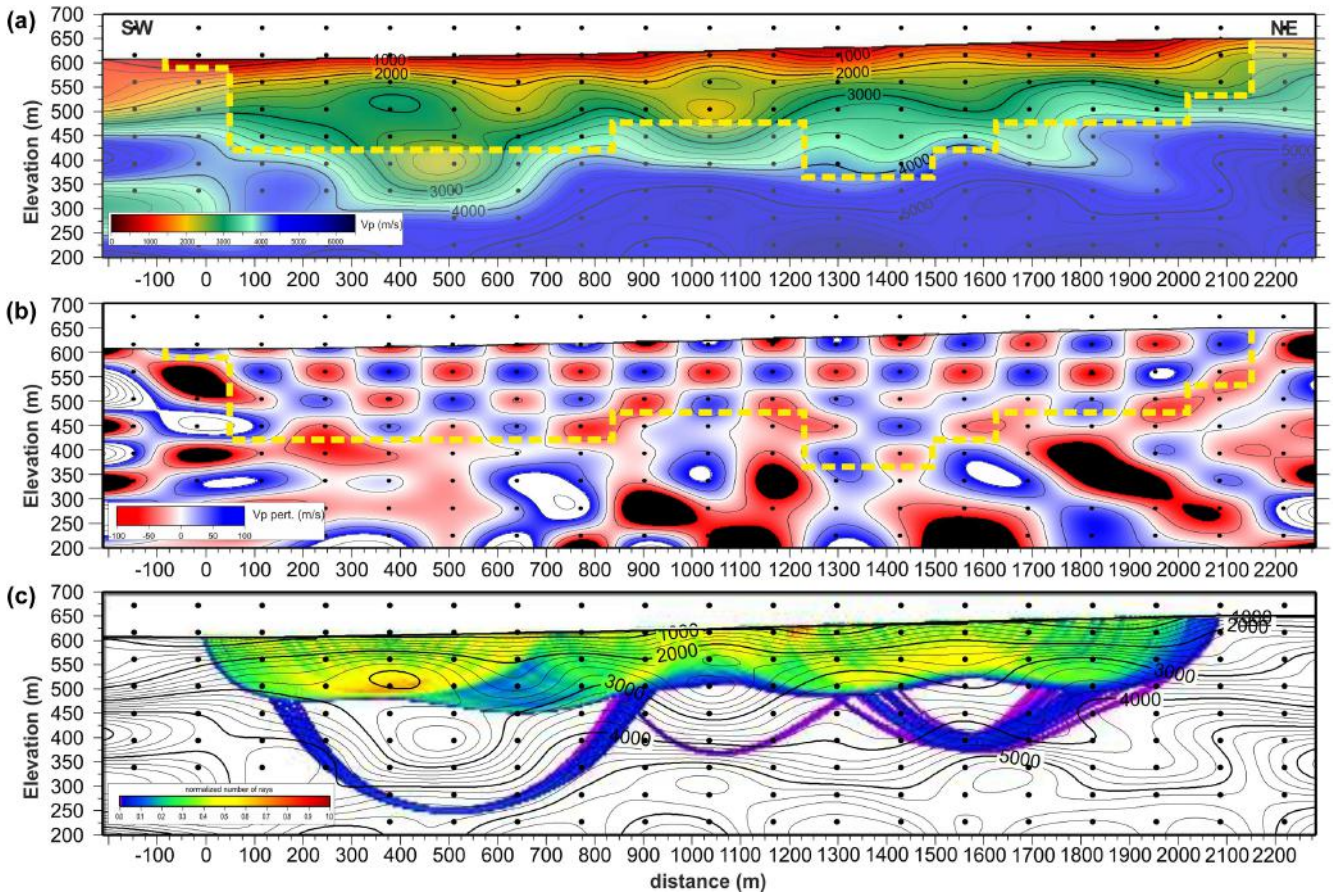

Figure 6. (a) Long-wavelength (171 parameters) *Vp* tomogram of profile P2: the dashed yellow line indicates resolution depth; (b) result of checkerboard test and (c) ray-density plot (normalized inside 5 m × 5 m cells).

lateral velocity contrasts, together with the thickening of low-*Vp* regions. This information is further cross-checked with evidence from known surface structures that we projected onto the tomograms.

We thus infer the occurrence of nine subsurface normal fault zones (labelled F1–F9) dipping both to the SW and to the NE (Fig. 10). This complex arrangement has already been recognized as a persistent structural feature of the Middle Aterno Valley at the surface and at different scales (Fig. 2c; Civico *et al.* 2015; Pucci *et al.* 2015, 2016; Villani *et al.* 2015b). Since an exact evaluation of fault dip from the inspection of the smooth tomographic images is difficult, in our interpretation we indicate fault zones with double dashed lines, assuming that average dip angles of ∼60° (SW-dipping) and ∼70° (NE-dipping) measured along outcrops (Section 2.2) are the same for the SW-dipping and NE-dipping buried fault zones, respectively. In the following, we describe these fault zones referring both to their tomographic image (Fig. 9) and to their final interpretation (Fig. 10).

The short-wavelength tomogram of profile P1 (Figs 8a and 9c) clearly images a >50-m-wide fault zone (labelled as F1) whose surface projection matches pretty good the master fault bounding the Quaternary basin to the NE (Fig. 2a; red arrows at 870 m in Fig. 9b and at 470 m in Fig. 9c). In the tomograms (Figs 9b and c), the presence of a SW-dipping normal fault is documented by the abrupt SW-deepening of the high-velocity basement and concurrent SW-thickening of the near-surface very-low velocity region ($Vp < 1000$ m s^{-1}). The short-wavelength tomogram also details the upper part of the fault zone, which can be confidently traced up to the surface based on the thickening of the $Vp < 1000$ m s^{-1} wedge: this feature clearly indicates syn-tectonic deposition of loose material in the hangingwall of fault F1 possibly enhanced by Late Pleistocene—Holocene tectonic subsidence, as also highlighted by the palaeoseismological trenches opened across it by Cinti *et al.* (2011). Worthy to note, the primary coseismic ruptures observed in this part of the Paganica village (Boncio *et al.* 2010; Emergeo Working Group 2010; Fig. 2a) are organized in two parallel sets spaced ∼30 m apart (double black arrows at 830 m in Fig. 9b and at 430 m in Fig. 9c), and they occur ∼40 m to the SW of the projected trace of the master fault. This highlights the complexity of the coseismic rupture process and the considerable width of the active fault zone. For fault F1 we evaluate ∼110 m throw.

The retrieved fault zone F2 (Figs 9b and c) is related to an evident step in the top-basement and a thickening of the low-*Vp* region (<2000 m s^{-1}) in the 50–100 m depth range. Notwithstanding some uncertainty, the subsurface location of fault zone F2 is consistent with the projection of an active splay (red arrow at 140 m in Fig. 9c) recognized after the earthquake (Galli *et al.* 2010; Cinti *et al.* 2011; Pucci *et al.* 2015; Fig. 2a), and subsequently investigated through trenching by Moro *et al.* (2013). For this fault we evaluate ∼80 m throw.

The fault zone F4 imaged in our tomograms (Fig. 9a) is a good candidate to represent the NW prolongation of the San Gregorio Fault (SGF in Fig. 2a) as previously mapped by Boncio *et al.* (2010) and Pucci *et al.* (2015). For this fault we evaluate ∼90 m throw.

The existence of a shallow blind fault in correspondence of fault zone F6 coincides with that hypothesized by Boncio *et al.* (2010) in the hangingwall of the SGF based on the occurrence of tensile

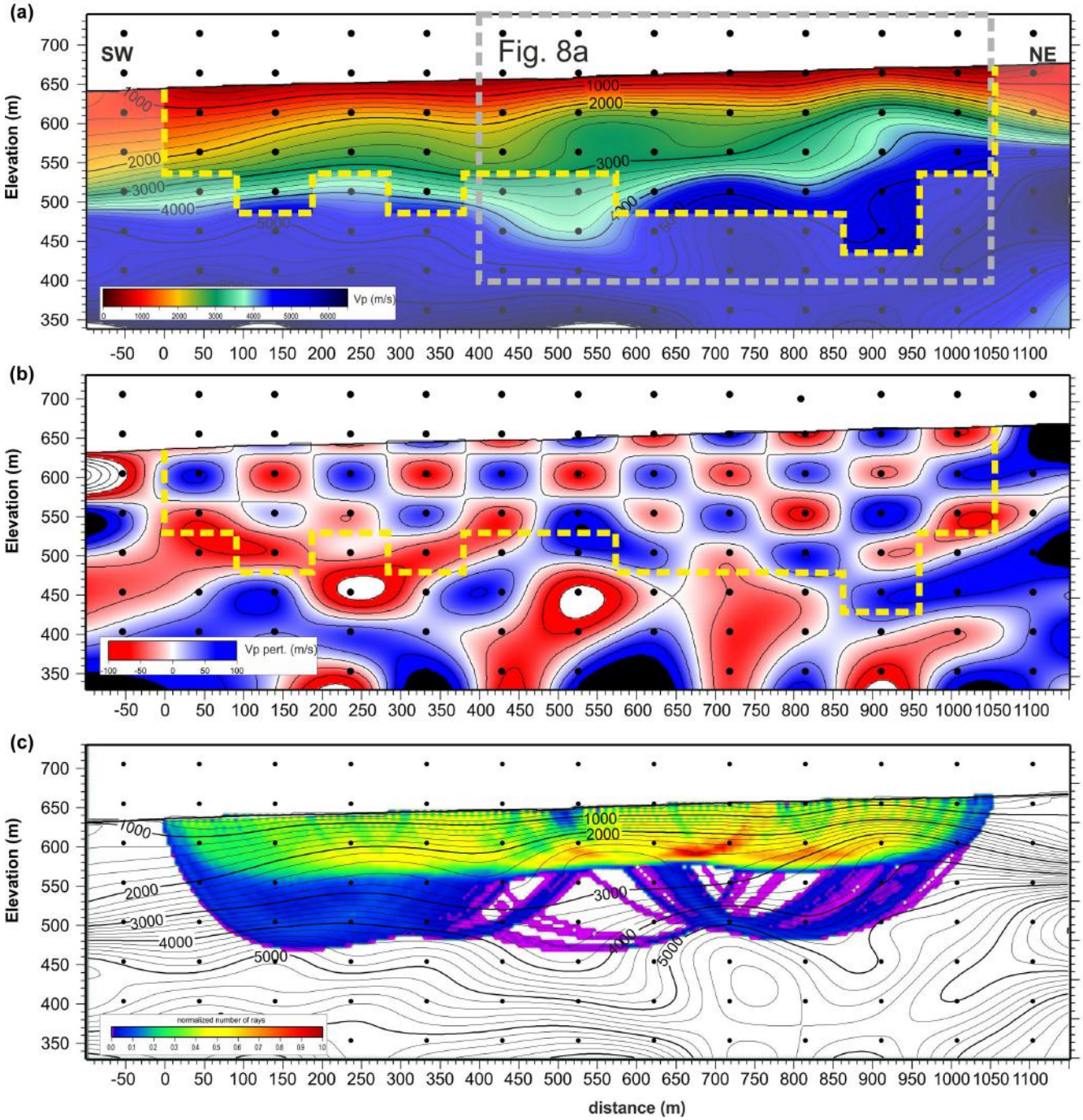

Figure 7. (a) Long-wavelength (104 parameters) *Vp* tomogram of profile P1: the dashed grey rectangle indicates the extent of the short-wavelength model shown in Fig. 8(a); the dashed yellow line indicates resolution depth; (b) result of checkerboard test and (c) ray-density plot (normalized inside 5 m × 5 m cells).

coseismic surface cracks (green stars in Figs 2a and 10). Hence, our subsurface fault image confirms previous speculations. For fault F6 we evaluate ∼75 m throw.

The remaining fault zones F3, F5, F7, F8 and F9 are detected for the first time in this study. The small fault zone F3, antithetic to F2, is located in a poorly resolved region of the tomograms (Figs 7a, 9b and 9c), however reflection data (cdp 183, labelled *e* in Figs 9 and S3) indicate the top-basement is located within the *Vp* 3800–4000 m s^{-1} zone between the two splays, thus defining a small graben.

Fault zones F7 and F8 bound the buried horst outcropping to the north as Mt Caticchio: the remarkable deepening of the basement suggests that the horst has a prominent plunge to the SE, or is probably down-faulted by a transversal structure. According to our interpretations, fault zone F7 has ∼90 m throw and fault zone F8 ∼120 m throw, so that Mt Caticchio separates two important depocentres in the Paganica basin, which are ∼280 and ∼250 m deep, respectively. This horst can be considered the more external portion of the Mt Bazzano structure, antithetic to the Paganica Fault.

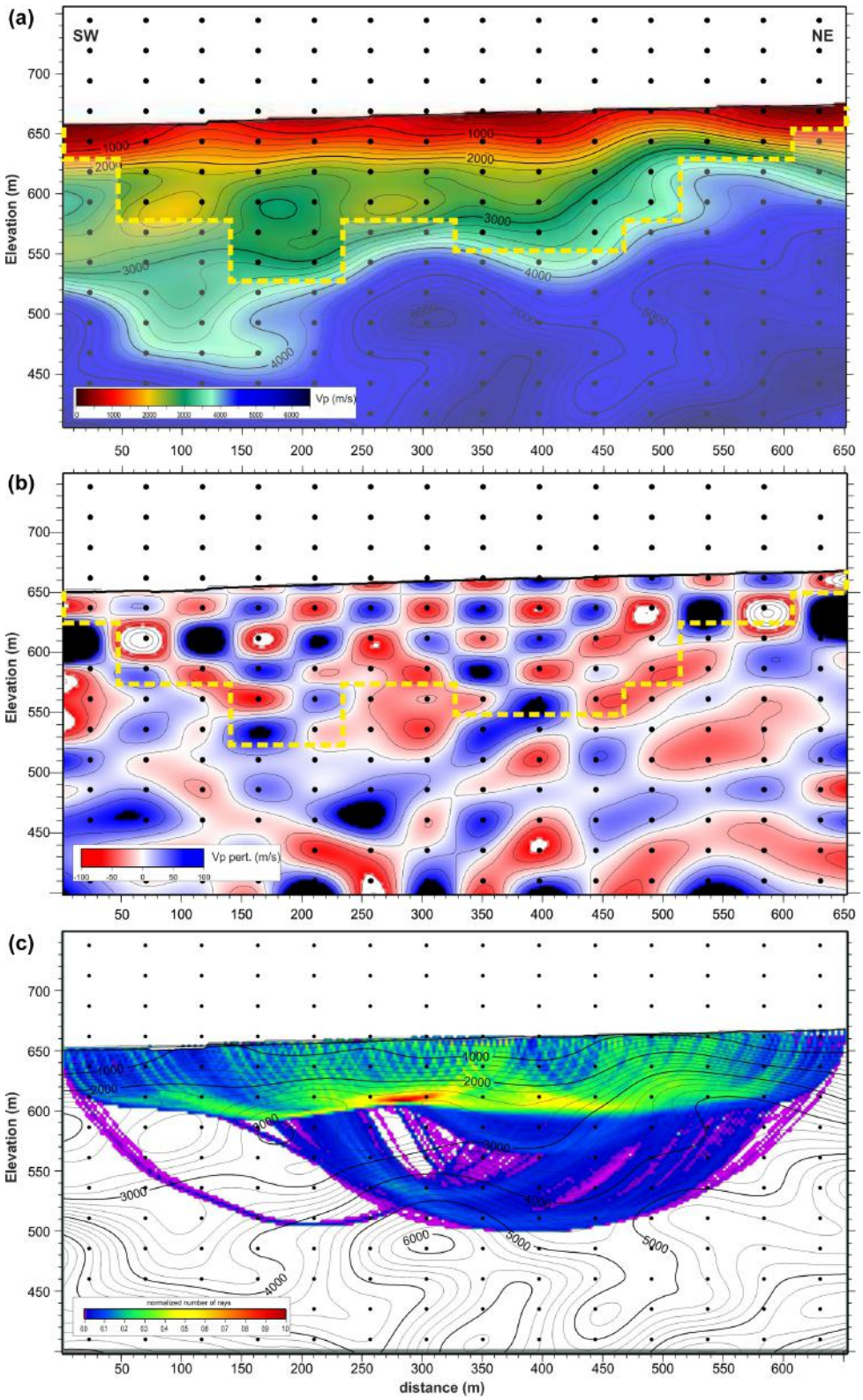

Figure 8. (a) Short-wavelength (196 parameters), high-resolution *Vp* tomogram of profile P1: the dashed yellow line indicates resolution depth; (b) result of checkerboard test and (c) ray-density plot (normalized inside 5 m × 5 m cells).

In the following, we name *Paganica fault-system* this kinematically coherent array of 12 synthetic and antithetic splays (BzF, F1–F9, PgF1 and PgF2) bounding and dissecting the Paganica basin.

6 DISCUSSION AND GEOLOGICAL IMPLICATIONS

The integrated cross-section A–A′ shown in Fig. 10 (trace reported in Fig. 2a) covers the entire width of the Paganica basin and

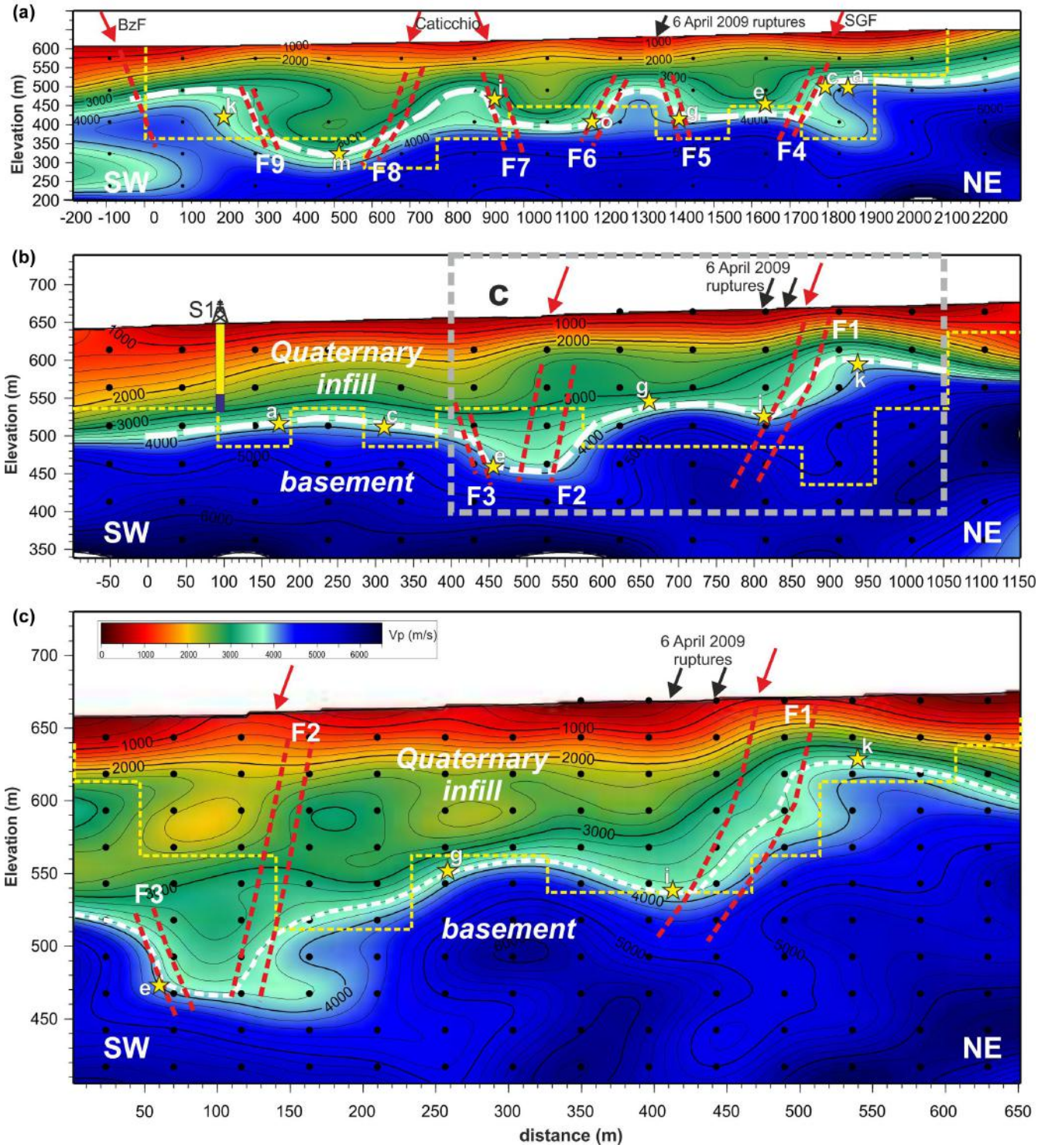

Figure 9. (a) Long-wavelength model of profile P2 with interpretation; (b) long-wavelength model of profile P1 with interpretation; (c) short-wavelength model of profile P1 with interpretation. The white dashed line indicates the top of the inferred pre-Quaternary basement; the yellow dashed line indicates resolution depth; the borehole S1 (projected 380 m from the SE) is also shown, the labelled yellow stars indicate reflection points of the top-basement inferred from depth-conversion of reflection arrivals from CMP gathers (details in Figs S3 and S4). The main fault zones are represented with dashed double lines and are thoroughly discussed in Section 5. Red arrows indicate the projection of the main outcropping faults. Black arrows indicate the 2009 April 6 coseismic surface breaks. Note that the three panels are drawn with different scales, due to the different length of profiles P1 and P2.

intersects most of the NW-trending splays affecting Quaternary deposits. It is 4.2 km long and is slightly shifted to the SE with respect to the seismic profiles, in order to be tied to the bedrock outcrops and the main bounding faults of the Paganica basin (BzF to the SW; PgF1 and PgF2 to the NE; Fig. 2a). For elementary geometric relations, in the hangingwall of fault F1 the basement cannot be older than the BIS *Fm.* (Section 5.1). Conversely, the basement in the hangingwall of fault BzF is less constrained, therefore we propose

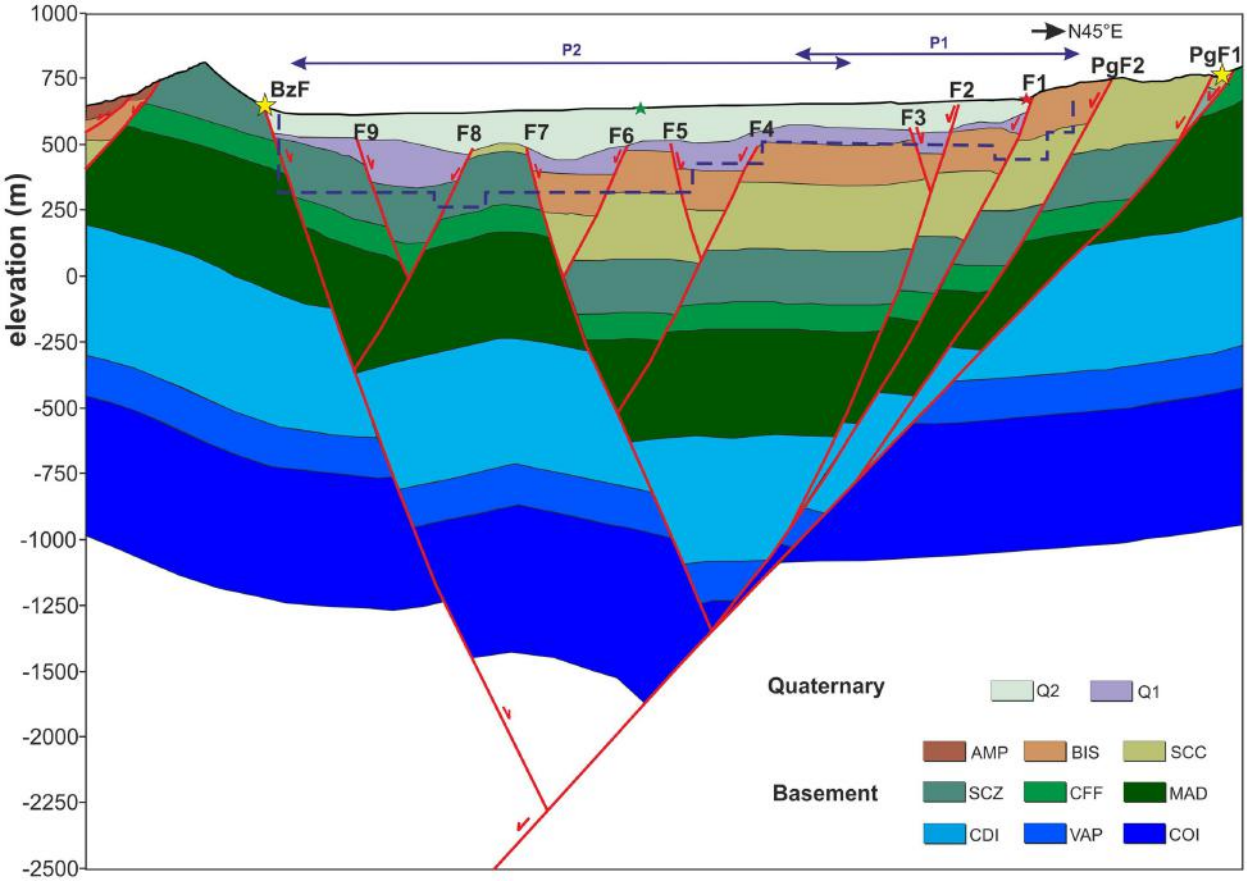

Figure 10. Geological cross-section A–A′ (trace shown in Fig. 2a) from the interpretation of the merged seismic profiles P1 and P2 (their extent is indicated by double blue arrows). Q1: alluvial fan deposits and breccia (MBR, VVC, VVB and VIC *Fms.*). Q2: fluvial and alluvial fan deposits (AFH, AFP and SMA *Fms.*). For the other acronyms refer to the caption of Fig. 2(a). The red star close to fault F1 indicates location of primary coseismic surface breaks at Paganica village, while the green star above fault F6 indicates secondary surface breaks (see details in the text). The thin black dashed line indicates the approximate investigation depth of the long-wavelength tomograms (Figs 9a and b). The yellow stars are the two piercing points used for the evaluation of extension (see Section 6). Faults BzF, PgF1 and PgF2 (see Fig. 2a), although not investigated by seismic profiles, are included in the section because they bound the overall half-graben.

an interpretation where it is represented by the SCZ *Fm*. (Fig. 10): this choice minimizes slip on faults BzF and F8, and thus the overall extension along the investigated transect.

We validated this structural model by iterative block-restoration (using a tool available with the Midland Valley MOVE© software) and assuming quasi-planar shallow fault geometry, layer thickness preservation, and negligible beds rotation due to faulting. The resulting small inaccuracies (areal gaps or overlaps between the 14 fault blocks after restoration are <1 per cent) are used to assign ∼10 and ∼5 m error on throw and heave for each fault block, respectively. As described in Section 2.2, the few kinematic data collected on some limited portions of faults BzF and PgF1 (Figs 2e and f) suggest that the Paganica fault-system exhibits an almost pure dip-slip kinematics (see also: Lavecchia *et al.* 2012), so we infer that the apparent displacement measured along this section is nearly equal to the net displacement. This further implies that our estimates of fault slip represent a minimum.

Since no geological constraint is available on the palaeo-topography pre-dating the basin formation, we also assume that the bumpy morphology of the top-bedrock is due to normal faulting: this is consistent with the evidence of a quite small amount of shortening due to thrusting in the study area, and with geological data indicating that extensional tectonic activity likely begun more than 1.8 Ma (Section 2.2). Worthy to note, along the Paganica fault-system we did not find any meso-structural evidence of inversion of older thrust surfaces (Fig. 2), which may support the hypothesis that the Paganica Fault re-activated a high-angle thrust developed on an earlier Mesozoic normal fault (Speranza & Minelli 2014; see Section 2.1).

6.1 Faults displacement

In order to calculate the total displacement of the investigated fault-system, we first measured the separation of footwall and hanging-wall cut-offs of the shallowest pre-Quaternary markers, namely the top of the SCZ, BIS and SCC *Fms.* in the SW, central, and NE parts of the section, respectively. We then checked the consistency of displacement across each fault splay down to the J–K units, although the setting of the central part of the section at greater depth (>500 m below the sea level, including the CDI, VAP and COI *Fms.* in Fig. 10) is less constrained. Subsequently, we summed separately the throws of SW-dipping and NE-dipping splays: the cumulative values obtained are ∼1220 m (for SW-dipping splays) and ∼845 m (for NE-dipping splays), resulting in a net throw of ∼375 m. Following the same approach, we summed separately the heave of SW-dipping and NE-dipping splays, obtaining ∼765 and ∼235 m, respectively. Finally, taking into account the aforementioned

geometric inaccuracies of the cross-section, the net displacement, throw and heave of the Paganica fault-system are 645 ± 90, 375 ± 60 and 530 ± 65 m, respectively. Since the distance between the piercing points of the section is 3.6 km, this implies ∼15 per cent stretching. These values confirm that in this sector of the central Apennines the extension is driven by an overall SW-dipping fault-system.

This geometric solution depicts the partitioning of fault slip within the uppermost ∼2 km of the crust with tolerable errors. In fact, if we consider the net displacement affecting the lowermost stratigraphic level in the section (base of COI *Fm.*), we still obtain ∼650 m of slip accrued by fault PgF1 at ∼2 km depth: this value is almost equal to the net displacement obtained considering the slip occurring along the 12 conjugate shallowest splays.

We conclude that a reliable minimum estimate of cumulative displacement of the Paganica Fault is 650 ± 90 m: such a value is higher than previous calculations of total offset (e.g. Galli *et al.* 2010; Improta *et al.* 2012). Interestingly, the minimum value of net throw of the Paganica Fault (∼375 ± 60 m) is roughly comparable with the 250–300 m total morphologic throw obtained by Civico *et al.* (2015). This implies that a large proportion of fault throw directly caused the offset of the topographic surface with the generation of a basin-and-range landscape. A further important implication is that such a kind of fault architecture (i.e. slip mostly localized on 60°-dipping synthetic splays and subordinately on a few 70°-dipping antithetic splays) requires a relatively low amount of net throw to generate a significant extension. For instance, Villani *et al.* (2015b) already documented a similar structural setting along the San Demetrio sector of the PSDFS.

6.2 Upper crustal architecture

The cross-section of Fig. 11 shows our interpretation of the possible link between the shallow structure (∼300 m) and the deep (>2 km) setting.

A simple extrapolation of planar geometry at depth suggests that faults F2–F9 are very shallow (<1 km), while faults PgF1, PgF2 and F1 intersect the main antithetic fault BzF at ∼2 km depth. The aftershocks of the 2009 M_w 6.1 L'Aquila earthquake align on a primary SW-dipping plane, which connects with the extrapolated prolongation at deep of faults PgF1, PgF2 and F1. We remark that the downward continuation of fault F1 inferred by refraction tomography (Fig. 8) also matches the seismogenic fault unravelled by aftershocks distribution. Therefore, our results indicate that the 2009 coseismic surface faulting occurred along a normal fault splay that displaces the pre-Quaternary basement with ∼110 m throw, and affects the whole overlying continental sequence up to the surface through repeated large earthquakes. In particular, from a structural point of view fault F1 plays the role of the master fault of the Quaternary Paganica basin, whereas fault PgF1 represents the *break-away* fault of the overall Paganica fault-system.

Moreover, our data support the hypothesis that the NW part of the San Gregorio Fault (SGF) together with its main synthetic splay (F6 in Figs 9 and 10) intersect fault F7 at very shallow depth, in the hangingwall of faults F1 and PgF1: this is consistent with the surface arrangement of the Paganica fault-system, made of two leading and right-stepping fault sets (PgF1, PgF2, F1 and F2 to the NW and SGF to the SE in Fig. 2a), with an overall length of ∼8 km. This length value represents a minimum because of the difficulty of accurately mapping the tips of the investigated fault-system, particularly in the case of the SE portion of the SGF.

Summarizing, in our interpretation (Fig. 11) the Paganica Fault is the 2009 seismogenic planar normal fault cutting the whole upper ∼10 km of the crust, and splaying out to the surface into a dozen shallow (<2 km deep) minor splays. This fault-system accrued a minimum 650 ± 90 m cumulative displacement, generating a ∼3-km-wide, asymmetrical continental basin, with a maximum infill thickness of ∼280 m (Paganica basin) bounded by prominent cumulative fault scarps on both sides.

As mentioned earlier in Section 2.1, the tectonic model recently proposed by Bonini *et al.* (2014) scales the Paganica Fault back to a shallow, secondary structure rooted at ∼3 km depth onto a gently dipping thrust surface preventing any upward propagation of the coseismic rupture. Provided that the authors did not quantify the net geological displacement of the Paganica Fault, the results of our work cast some doubt on this model, since: (1) the 2009 coseismic ruptures occurred along a large-displacement, mature Quaternary normal fault (Figs 2a and 10) showing evidence of surface-rupturing palaeo-earthquakes (Section 2.1) and clearly displacing the pre-Quaternary basement (Figs 9b and c); (2) the uppermost portion of the Paganica Fault is almost perfectly aligned with the 2009 aftershocks in the 2–10 km depth range (Fig. 11); (3) the Paganica fault-system, together with the SGF, forms an >8-km-long individual structure at the surface (Fig. 2a). Notably, our minimum estimate of net displacement of the Paganica Fault is in accordance with fault length/displacement scaling relationships (e.g. Kim & Sanderson 2005, and reference therein) from field data collected on many other normal faults worldwide. Moreover, the interpretation of a normal fault cutting the uppermost ∼10 km of the crust is consistent with the evidence that most inter-plate dip-slip seismogenic faults have an aspect ratio of ∼1 (Leonard 2010).

6.3 Short-term versus long-term slip-rates of the Paganica fault-system

We use the mutual relations between faults and continental infill in Fig. 10 to infer long-term (>10^5 yr timescale) slip-rates of the Paganica fault-system. The continental deposition in the Paganica basin likely took place during the Gelasian (1.8–2.59 Ma; Section 2). Taking into account the uncertainty in the onset of extension and the aforementioned inaccuracies affecting slip calculation, the minimum long-term slip-rate is 0.30 ± 0.07 mm yr^{-1}. Such value falls within the reported 0.2–1.3 mm yr^{-1} range of slip-rates for active normal faults in the central Apennines (Section 1), which consider shorter timescales (typically 10^3 yr), and are close to the dip-slip rates of 0.3–0.4 mm yr^{-1} recovered from palaeoseismic surveys across splays F1 and F2 (Cinti *et al.* 2011; Galli *et al.* 2011; Moro *et al.* 2013). As regards total extension, we evaluate a 0.25 ± 0.06 mm yr^{-1} minimum long-term extension-rate accomplished by the whole Paganica fault-system at the surface.

Based on the relationships between faults and infilling deposits Q1 and Q2 in the Paganica basin (Fig. 10), we hypothesize that post-Early Pleistocene activity of the Paganica fault-system is basically accomplished by faults F1 (master), F2, and subordinately by faults BzF, F4 and F6, whereas all the other splays appear sealed since the beginning of the Middle Pleistocene. Therefore, within the Paganica fault-system a spatio-temporal migration of activity likely occurred, causing higher concentration of slip in recent times over a few splays and contemporaneous deactivation of the other splays. This

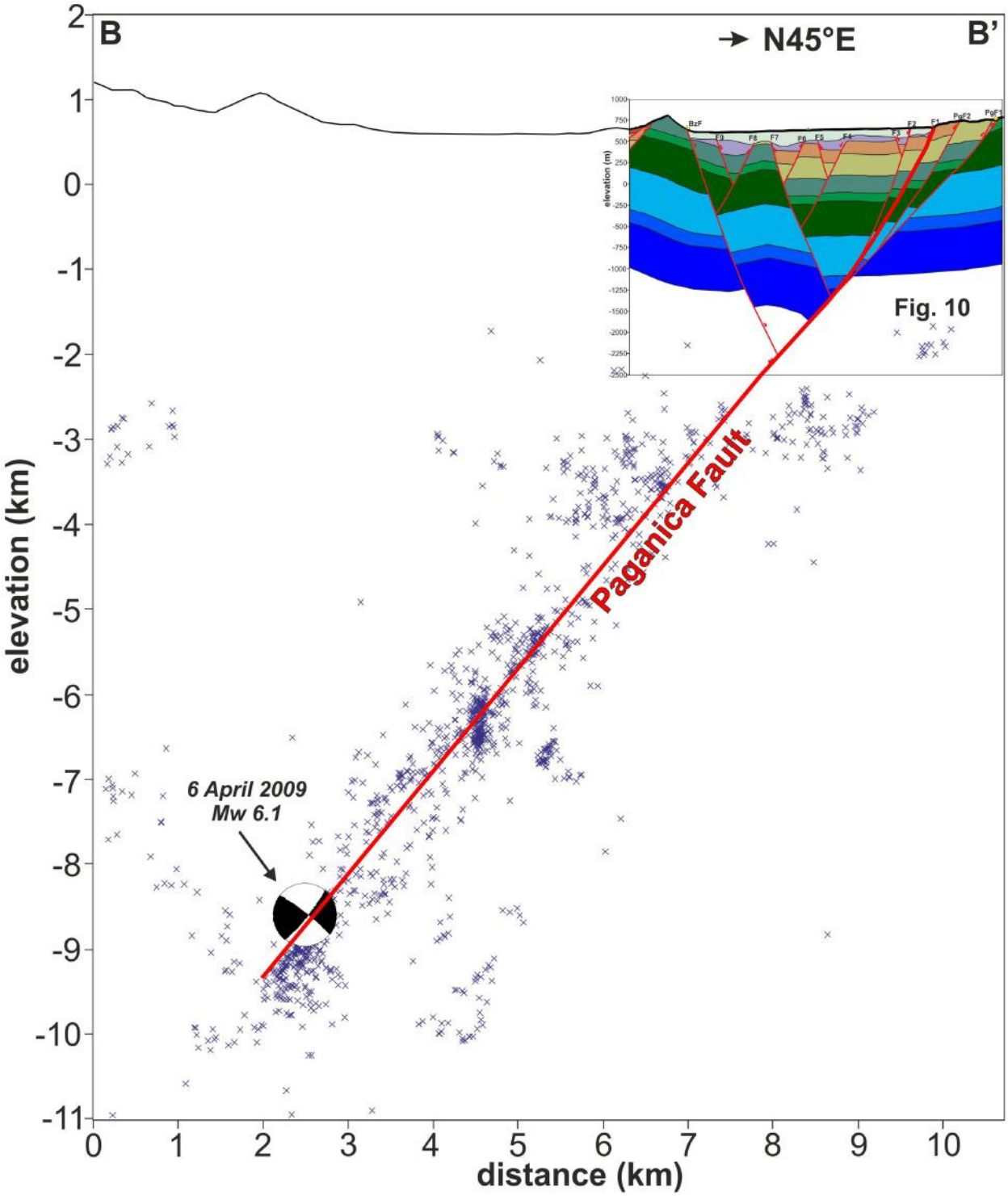

Figure 11. Cross-section B–B′ (trace shown in Fig. 1) with the projection of the 2009 April 6 main shock focal mechanism and 1343 high-precision relocated aftershocks (small blue crosses; 1 km width perpendicular to the section; dataset after: Valoroso *et al.* 2013). In the upper part, the geological section of Fig. 10 is shown. Simple extrapolation downwards of planar fault surfaces implies that the Paganica half-graben structure is quite shallow, with conjugate splays merging at ∼2 km depth.

time-dependent scenario, which has occurred at upper structural levels (0–2 km deep), is consequently the surface expression of the displacement occurring at seismogenic depth along a single SW-dipping master fault (Paganica Fault).

Several works (Nicol *et al.* 1997, 2006; Cowie 1998; Bull *et al.* 2006; Mouslopoulou *et al.* 2009) have documented that, given steady-state boundary conditions, kinematically coherent normal fault-systems accrue displacement at nearly constant rate and approach stability over a time-interval $>10^3$ yr. Similarly, from the aggregate contribution of all the splays composing the fault-system investigated in this work, we infer that displacement of the Paganica Fault accrued in a stable manner in the long-term perspective.

As a final remark, we put forward the hypothesis that the Paganica fault-system behaves as a first-order crustal structure, similar to a few other active normal fault-systems depicted in Fig. 1, in particular those faults that are nearly parallel to the PSDFS along the direction of regional extension (e.g. the Liri, Velino-Magnola, L'Aquila-Celano and Gran Sasso fault-systems). Considering that in the last 1.2–1.8 × 10^4 yr the averaged regional extension-rate accomplished by all of these faults in the axial zone of the central Apennines is ∼1 mm yr^{-1} (Faure Walker *et al.* 2010), we argue that at comparable timescales (10^4–10^5 yr) the Paganica fault-system may account for ∼20 per cent of the total extension affecting this part of the chain.

7 CONCLUSIONS

The integration of HR *Vp* tomographic images and detailed geological mapping allowed the reconstruction of the architecture of the shallow portion of the Paganica Fault, which is the source of the 2009 M_w 6.1 L'Aquila earthquake (Figs 10 and 11). Our *Vp* images pinpoint the shallow geometry of this previously poorly known normal fault (that was also responsible of heavy damage caused by co-seismic surface breakage), moreover several buried fault splays were recognized for the first time by using this new set of data. This fact highlights that HR seismic profiling integrated with detailed geological mapping should be considered as a primary tool to use for subsurface basin imaging and assessing surface faulting hazard in complex tectonic scenarios.

The Paganica fault-system is composed of 12 main conjugate splays dipping to the SW and to the NE, which accrued a minimal total displacement of 650 ± 90 m, accounting for a long-term (post-Gelasian) slip-rate of 0.30 ± 0.07 mm yr^{-1}. Similarly, the overall extension is 530 ± 65 m, accounting for a long-term extension-rate of 0.25 ± 0.06 mm yr^{-1}. The total net throw of 365 ± 60 m is comparable to previous estimates of total morphologic throw (Civico *et al.* 2015), suggesting that this fault played a primary role in generating a basin-and-range landscape.

Extension promoted the formation of a ∼3-km-wide half-graben (Paganica basin). The infill thickness is extremely variable, ranging between <20 m and a maximum value of ∼280 m. *Vp* images suggest in the hangingwall of each fault the presence of thick syntectonic clastic wedges (unit Q1), which developed during early extensional phases promoting the basin formation.

We infer that normal fault activity during the Early Pleistocene involved all of the fault splays, whereas the post-Early Pleistocene displacement was accrued by three main splays (the master fault F1, and faults F2 and BzF) and to a much lesser extent by two other minor splays (F4 and F6).

We hypothesize that at 10^4–10^5 yr timescales the Paganica fault-system, together with a few other parallel active normal fault-systems in the axial zone of the central Apennines (e.g. the Liri, Velino-Magnola, L'Aquila-Celano and Gran Sasso fault-systems), behaves as a first-order structure cutting the whole upper ∼10 km of the crust, and which accounts for ∼20 per cent of the total extension affecting this part of the chain.

The integrated subsurface investigation of the Paganica Fault presented in this work improves the knowledge of the Late Quaternary structural evolution of this highly seismic sector of the central Apennines, and it represents a pinpoint for the thorough characterization of an active fault-system at different timescales and structural levels in the crust.

ACKNOWLEDGEMENTS

Two anonymous reviewers provided thoughtful comments that greatly improved the early version of this manuscript. We also thank the editor J. Virieux for his positive remarks on this paper, and M. Carafa, D. Di Naccio and A. Herrero for fruitful discussions.

Seismic data have been processed using the Seismic Unix Package (Stockwell 1999). Tomographic models have been plotted with the Generic Mapping Tool software (Wessel & Smith 1991). The geological cross-section was created using the Midland Valley Software MOVE© (http://www.mve.com/software; academic licence 2016 for INGV, Rome). L. Valoroso provided the aftershocks locations and D. Cheloni the focal mechanism shown in Fig. 11.

This work has been funded by the Project INGV-DPC S5 07–09 '*Test sites per il monitoraggio multidisciplinare di dettaglio*' W.P. 4.5, (team 0371.050, UR8, P.I.: L. Improta,) and by the Project FIRB Abruzzo '*High-resolution analyses for assessing the seismic hazard and risk of the areas affected by the 6 April 2009 earthquake*' (http://progettoabruzzo.rm.ingv.it/en; UR5, P.I.: D. Pantosti; funding code: RBAP10ZC8K_005).

REFERENCES

Akinci, A., Galadini, F., Pantosti, D., Petersen, M., Malagnini, L. & Perkins, D., 2009. Effect of time dependence on probabilistic seismic-hazard maps and deaggregation for the Central Apennines, Italy, *Bull. seism. Soc. Am.,* **99**(2A), 585–610.

An, M., 2012. A simple method for determining the spatial resolution of a general inverse problem, *Geophys. J. Int.,* **191**(2), 849–864.

Atzori, S. *et al.*, 2009. Finite fault inversion of DInSAR coseismic displacement of the 2009 L'Aquila earthquake (central Italy), *Geophys. Res. Lett.,* **36,** L15305, doi:10.1029/2009GL039293.

Bagh, S., Chiaraluce, L., De Gori, P., Moretti, M., Govoni, A., Chiarabba, C., Di Bartolomeo, P. & Romanelli, M., 2007. Background seismicity in the Central Apennines of Italy: the Abruzzo region case study, *Tectonophysics,* **444,** 80–92.

Bagnaia, R., D'Epifanio, A. & Sylos Labini, S., 1992. Aquila and subaequan basins: an example of Quaternary evolution in central Apennines, Italy, *Quat. Nova,* II, 187–209.

Balasco, M. *et al.*, 2011. Deep geophysical electromagnetic section across the middle Aterno Valley (central Italy): preliminary results after the April 6, 2009 L'Aquila earthquake, *Boll. Geofis. Teor. Appl.,* **52**, 443–455.

Benedetti, L. *et al.*, 2013. Earthquake synchrony and clustering on Fucino faults (Central Italy) as revealed from in situ 36Cl exposure dating, *J. geophys. Res.,* **118,** 4948–4974.

Bertini, T. & Bosi, C., 1993. La tettonica quaternaria della conca di Fossa – San Demetrio (L'Aquila), *Il Quaternario (Ital. J. Quarter. Sci.),* **6**(2), 293–314.

Bigi, S., Casero, P. & Ciotoli, G., 2011. Seismic interpretation of the Laga basin; constraints on the structural setting and kinematics of the Central Apennines, *J. Geol. Soc.,* **168**(1), 1–11.

Blumetti, A.M., Guerrieri, L. & Vittori, E., 2013. The primary role of the Paganica-San Demetrio fault system in the seismic landscape of the Middle Aterno Valley basin (Central Apennines), *Quarter. Int.,* **288,** 183–194.

Blumetti, A.M., Di Manna, P., Vittori, E., Comerci, V. & Guerrieri, L., 2015. Paleoseismicity data on the San Demetrio ne' Vestini fault (L'Aquila Basin, Central Italy), Abstracts Volume 6th International INQUA Meeting on Paleoseismology, Active Tectonics and Archaeoseismology. 19 | 24 April 2015, Pescina, Fucino Basin, Italy (eds Blumetti, A.M., Cinti, F.R., De Martini, P.M., Galadini, F., Guerrieri, L., Michetti, A.M., Pantosti, D. & Vittori, E.), Miscellanea INGV, 27, 511-513, ISSN: 2039-6651.

Boncio, P., Lavecchia, G. & Pace, B., 2004. Defining a model of 3D seismogenic sources for seismic hazard assessment applications: the case of central Apennines (Italy), *J. Seismol.,* **8**(3), 407–425.

Boncio, P., Pizzi, A., Brozzetti, F., Pomposo, G., Lavecchia, G., Di Naccio, D. & Ferrarini, F., 2010. Coseismic ground deformation of the 6 April 2009 L'Aquila earthquake (central Italy, Mw6.3), *Geophys. Res. Lett.,* **37,** L06308, doi:10.1029/2010GL042807.

Bonini, L., Di Bucci, D., Toscani, G., Seno, S. & Valensise, G., 2014. On the complexity of surface ruptures during normal faulting earthquakes: excerpts from the 6 April 2009 L'Aquila (central Italy) earthquake (Mw 6.3), *Solid Earth,* **5,** 1–19.

Bosi, C., Galadini, F., Giaccio, B., Messina, P. & Sposato, A., 2003. Plio-Quaternary continental deposits in the Latium-Abruzzi Apennines: the correlation of geological events across different intermontane basins, *Il Quaternario (Ital. J. Quarter. Sci.),* **16**(1bis), **2003,** 55–76.

Bruno, P.P., Improta, L., Castiello, A., Villani, F. & Montone, P., 2010a. The Vallo di Diano Fault System: new evidence for an active range-bounding fault in southern Italy using shallow, high-resolution seismic profiling, *Bull. seism. Soc. Am.: Short Notes,* **100**(**2**), doi:10.1785/0120090210.

Bruno, P.P., Castiello, A. & Improta, L., 2010b. Ultrashallow seismic imaging of the causative fault of the 1980, M6.9, southern Italy earthquake by pre-stack depth migration of dense wide-aperture data. *Geophys. Res. Lett.,* **37,** L19302, doi:10.1029/2010GL044721.

Bruno, P.P., Castiello, A., Villani, F. & Improta, L., 2013. High-resolution densely spaced wide-aperture seismic profiling as a tool to aid seismic hazard assessment of fault-bounded intramontane basins: application to Vallo di Diano, Southern Italy, *Bull. seism. Soc. Am.,* **103**(3), 1969–1980.

Bull, J.M., Barnes, P.M., Lamarche, G., Sanderson, D.J., Cowie, P.A., Taylor, S.K. & Dix, J.K., 2006. High-resolution record of displacement accumulation on an active normal fault: implications for models of slip accumulation during repeated earthquakes, *J. Struct. Geol.,* **28,** 1146–1166.

Calvert, A.J. & Fisher, M.A., 2001. Imaging the Seattle fault zone with high-resolution seismic tomography, *Geophys., Res. Lett.,* **28**(12), 2337–2340.

Carafa, M.M.C., Barba, S. & Bird, P., 2015. Neotectonics and long-term seismicity in Europe and the Mediterranean region, *J. geophys. Res.,* **120,** doi:10.1002/2014JB011751.

Catchings, R.D., Gandhok, G., Goldman, M.R., Okaya, D., Rymer, M.-J. & Bawden, G.W., 2008. Near-surface location, geometry and velocity of the Santa Monica fault zone, Los Angeles, *Bull. seism. Soc. Am.,* **98,** 124–138.

Cavinato, G.P. & De Celles, P.G., 1999. Extensional basins in the tectonically bimodal central Apennines fold-thrust belt, Italy: response to corner flow above a subducting slab in retrograde motion, *Geology,* **27**(10), 955–958.

Cavinato, G.P., Carusi, C., Dall'Asta, M., Miccadei, E. & Piacentini, T., 2002. Sedimentary and tectonic evolution of Plio-Pleistocene alluvial and lacustrine deposits of Fucino Basin (central Italy), *Sediment. Geol.,* **148**(1), 29–59.

Centamore, E. *et al.*, 2006. Note illustrative della Carta Geologica d'Italia alla scala 1:50.000, Foglio 359 "L'Aquila". APAT – Servizio Geologico d'Italia e Regione Abruzzo – Servizio Difesa del Suolo, S.EL.CA., Firenze, 2006, 128 pp.

Chiarabba, C., Jovane, L. & Di Stefano, R., 2005. A new view of Italian seismicity using 20 years of instrumental recordings, *Tectonophysics,* **305,** 251–268.

Chiarabba, C. *et al.*, 2009. The 2009 L'Aquila (central Italy) M_W6.3 earthquake: main shock and aftershocks, *Geophys. Res. Lett.,* **36,** L18308, doi:10.1029/2009GL039627.

Chiarabba, C. & Chiodini, G., 2013. Continental delamination and mantle dynamics drive topography, extension and fluid discharge in the Apennines, *Geology,* **41,** 715–718.

Chiaraluce, L., 2012. Unraveling the complexity of Apenninic extensional fault systems: a review of the 2009 L'Aquila earthquake (Central Apennines, Italy), *J. Struct. Geol.,* **42,** 2–18.

Chiaraluce, L., Valoroso, L., Piccinini, D., Di Stefano, R. & De Gori, P., 2011. The anatomy of the 2009 L'Aquila normal fault system (central Italy) imaged by high resolution foreshock and aftershock locations, *J. geophys. Res.,* **116,** B12311, doi:10.1029/2011JB008352.

Cinti, F.R. *et al.*, 2011. Evidence for surface faulting events along the Paganica Fault prior to the 6 April 2009 L'Aquila earthquake (central Italy), *J. geophys. Res.,* **116** (B7), 2156–2202.

Cirella, A., Piatanesi, A., Tinti, E., Chini, M. & Cocco, M., 2012. Complexity of the rupture process during the 2009 L'Aquila, Italy, earthquake, *Geophys. J. Int.,* **190,** 607–621.

Civico, R., Pucci, S., Pantosti, D., De Martini, P.M. & Pantosti, D., 2015. Morphotectonic analysis of the long-term surface expression of the 2009 L'Aquila earthquake fault (Central Italy) using airborne LiDAR data, *Tectonophysics,* **644–645,** 108–121.

Cosentino, D., Cipollari, P., Marsili, P. & Scrocca, D., 2010. Geology of the central Apennines: a regional review, in *The Geology of Italy*, *Journal of the Virtual Explorer,* eds, Beltrando, M., Peccerillo, A., Mattei, M., Conticelli, S. & Doglioni, C., Electronic Edition. Available at: http://virtualexplorer.com.au/article/2009/223/apennines-review, last accessed June 2016.

Cowie, P.A., 1998. A healing-reloading feedback control on the growth rate of seismogenic faults, *J. Struct. Geol.,* **20**(8), 1075–1087.

Cowie, P.A. & Roberts, G.P., 2001. Constraining slip rates and spacings for active normal faults, *J. Struct. Geol.,* **23,** 1901–1915.

D'Agostino, N., Chamot-Rooke, N., Funiciello, R., Jolivet, L. & Speranza, F., 1998. The role of pre-existing thrust faults and topography on the styles of extension in the Gran Sasso range (Central Italy), *Tectonophysics,* **292,** 229–254.

D'Agostino, N., Jackson, J.A., Dramis, F. & Funiciello, R., 2001. Interactions between mantle upwelling, drainage evolution and active normal faulting: an example from the central Apennines (Italy), *Geophys. J. Int.,* **147**(2), 475–497.

D'Agostino, N., Avallone, A., Cheloni, D., D'Anastasio, E. & Mantenuto, S., 2008. Active tectonics of the Adriatic region form GS and earthquake slip vectors, *J. geophys. Res.,* **113,** B12413, doi:10.1029/2008JB005860.

D'Amico, S., Koper, K.D., Herrmann, R.B., Akinci, A. & Malagnini, L., 2010. Imaging the rupture of the Mw 6.3 April 6, 2009 L'Aquila, Italy earthquake using back-projection of teleseismic *P*-waves, *Geophys. Res. Lett.,* **37,** L03301, doi:10.1029/2009GL042156.

Devoti, R., Esposito, A. & Pietrantonio, G., 2011. Evidence of large scale deformation patterns from GPS data in the Italian subduction boundary, *Earth planet. Sci. Lett.,* **311**(3–4), 230–241.

Dìaz, D., Maksymowicz, A., Vargas, G., Vera, E., Contreras-Reyes, E. & Rebolledo, S., 2014. Exploring the shallow structure of the San Ramòn thrust fault in Santiago, Chile (∼33.5°S), using active seismic and electric methods, *Solid Earth,* **5,** 837–849.

Emergeo Working Group, 2010. Evidence for surface rupture associated with the Mw 6.3 L'Aquila earthquake sequence of April 2009 (central Italy), *Terra Nova,* **22**(1), 43–51.

Falcucci, E. *et al.*, 2009. The Paganica Fault and surface coseismic ruptures caused by the 6 April 2009 earthquake (L'Aquila, central Italy), *Seism. Res. Lett.,* **80**(6), 940–950.

Falcucci, E., Gori, S., Moro, M., Pisani, A.R., Melini, D., Galadini, F. & Fredi, P., 2011. The 2009 L'Aquila earthquake (Italy): what's next in the region? Hints from stress diffusion analysis and normal fault activity, *Earth planet. Sci. Lett.,* **2011,** doi:10.1016/j.epsl.2011.03.016.

Faure Walker, J.P., Roberts, G.P., Sammonds, P.R. & Cowie, P., 2010. Comparison of earthquake strain rates over 10^2 to 10^4 year timescales: insights into variability in the seismic cycle in the central Apennines, Italy, *J. geophys. Res.,* **115,** B10418, doi:10.1029/2009JB006462.

Galadini, F. & Galli, P., 1999. The Holocene paleoearthquakes on the 1915 Avezzano earthquake faults (central Italy): implications for active tectonics in the central Apennines, *Tectonophysics,* **308,** 143–170.

Galadini, F. & Galli, P., 2000. Active tectonics in the central Apennines (Italy)—input data for seismic hazard assessment, *Nat. Hazards,* **22,** 225–270.

Galadini, F. & Galli, P., 2003. Paleoseismology of silent faults in the Central Apennines (Italy): the Mt. Vettore and Laga Mts. Faults, *Ann. Geophys.,* **46**(5), 815–836.

Galli, P., Galadini, F., Moro, M. & Messina, P., 2002. New paleoseismological data from the Gran Sasso d'Italia area (central Apennines), *Geophys. Res. Lett.,* **29**(7), 38-1–38-4.

Galli, P., Galadini, F. & Pantosti, D., 2008. Twenty years of paleoseismology in Italy, *Earth-Sci. Rev.,* **88**(1), 89–117.

Galli, P.A., Giaccio, B. & Messina, P., 2010. The 2009 central Italy earthquake seen through 0.5 Myr-long tectonic history of the L'Aquila faults system, *Quarter. Sci. Rev.,* **29**(27–28), 3768–3789.

Galli, P.A., Giaccio, B., Messina, P., Peronace, E. & Zuppi, G.M., 2011. Palaeoseismology of the L'Aquila faults (central Italy, 2009, Mw 6.3 earthquake): implications for active fault linkage, *Geophys. J. Int.,* **187**(3), 1119–1134.

Galli, P., Giaccio, B., Peronace, E. & Messina, P., 2015. Holocene paleoearthquakes and Early–Late Pleistocene slip rate on the Sulmona Fault (Central Apennines, Italy), *Bull. Soc. seism. Am.,* **105**(1), 1–13.

Ghisetti, F. & Vezzani, L., 1991. Thrust geometries and sequence of imbrication in the Gran Sasso Chain (Central Apennines, Italy), *Ital. J. Geosci.,* **110**(3-4), 427–440.

Ghisetti, F. & Vezzani, L., 1999. Depths and modes of Pliocene-Pleistocene crustal extension of the Apennines (Italy), *Terra Nova,* **11,** 67–72.

Giaccio, B. *et al.*, 2012. Fault and basin depocentre migration over the last 2 Ma in the L'Aquila 2009 earthquake region, central Italian Apennines, *Quarter. Sci. Rev.,* **56,** 69–88.

Giocoli, A., Galli, P., Giaccio, B., Lapenna, V., Messina, P., Peronace, E., Romano, G. & Piscitelli, S., 2011. Electrical Resistivity Tomography across the Paganica-San Demetrio fault system (L'Aquila 2009 earthquake), *Bull. Geofis. Teor. Appl.,* **52**(3), 457–469.

Giraudi, C., 1995. Considerations on the significance of some postglacial fault scarps in the Abruzzo Apennines (Central Italy), *Quarter. Int.,* **25,** 33–45.

Gori, S., Giaccio, B., Galadini, F., Falcucci, E., Messina, P., Sposato, A. & Dramis, F., 2011. Active normal faulting along the Mt. Morrone southwestern scope (central Apennines, Italy), *Int. J. Earth Sci.,* **100**(1), 157–171.

Hearn, T.M. & Ni, J.F., 1994. Pn velocities beneath continental collision zones: the Turkish-Iranian Plateau, *Geophys. J. Int.,* **117**(2), 273–283.

Herrmann, R.B., Malagnini, L. & Munafò, I., 2011. Regional moment tensors of the 2009 L'Aquila earthquake sequence, *Bull. seism. Soc. Am.,* **101,** 975–993.

Hustand, I., Selvaggi, G., D'Agostino, N., England, P., Clarke, P. & Pierozzi, M., 2003. Geodetic strain in peninsular Italy between 1875 and 2001, *Geophys. Res. Lett.,* **30**(4), 1181, doi:10.1029/2002GL016447.

Improta, L. & Bruno, P.P., 2007. Combining seismic reflection with multifold wideaperture profiling: an effective strategy for high-resolution shallow imaging of active faults, *Geophys. Res. Lett.,* **34,** L20310, doi:10.1029/2007GL031893.

Improta, L. & Corciulo, M., 2006. Controlled source non-linear tomography: a powerful tool to constrain tectonic models of the Southern Apennines orogenic wedge, Italy, *Geology,* **34**(11), 941–944.

Improta, L., Zollo, A., Herrero, A., Frattini, M., Virieux, J. & Dell'Aversana, P., 2002. Seismic imaging of complex structures by non-linear traveltime inversion of dense wide-angle data: application to a thrust belt, *Geophys. J. Int.,* **151,** 264–278.

Improta, L., Zollo, A., Bruno, P.P., Herrero, A. & Villani, F., 2003. High resolution seismic tomography across the 1980 (Ms 6.9) Southern Italy earthquake fault scarp, *Geophys. Res. Lett.,* **30**(10), 1494, doi:10.1029/2003GL017077.

Improta, L. *et al.*, 2010. Detecting young, slow-slipping active faults by geologic and multidisciplinary high-resolution geophysical investigations: a case study from the Apennine seismic belt, Italy, *J. geophys. Res.,* **115,** B11307, doi:10.1029/2010JB000871.

Improta, L. *et al.*, 2012. High-resolution controlled-source seismic tomography across the Middle Aterno basin in the epicentral area of the 2009, Mw 6.3, L'Aquila earthquake (central Apennines, Italy), *Ital. J. Geosci.,* **131**(3), 373–388.

Kim, Y.-S. & Sanderson, D.J., 2005. The relationships between displacement and length of faults: a review, *Earth-Sci. Rev.,* **68,** 317–334.

Lavecchia, G., Brozzetti, F., Barchi, M., Menichetti, M. & Keller, J.V.A., 1994. Seismotectonic zoning in east-central Italy deduced from an analysis of the Neogene to present deformations and related stress fields, *Geol. Soc. Am. Bull.,* **106,** 1107–1120.

Lavecchia, G., Ferrarini, F., Brozzetti, F., De Nardis, R., Boncio, P. & Chiaraluce, L., 2012. From surface geology to aftershock analysis: constraints on the geometry of the L'Aquila 2009 seismogenic fault system, *Ital. J. Geosci.,* **131**(3), 330–347.

Lebedev, S. & Nolet, G., 2003. Upper mantle beneath Southeast Asia from S velocity tomography, *J. geophys. Res.,* **108**(B1), 2048, doi:10.1029/2000JB000073.

Leonard, M., 2010. Earthquake fault scaling: self-consistent relating of rupture length, width, average displacement, and moment release, *Bull. seism. Soc. Am.,* **100**(5A), 1971–1988.

Lutter, W.J. & Nowack, R.L., 1990. Inversion for crustal structure using reflections from the PASSCAL Ouachita experiment, *J. geophys. Res.,* **95** (B4), 4633–4646.

Macrì, P., Smedile, A., Speranza, F., Sagnotti, L., Porreca, M., Mochales, T. & Russo Ermolli, E., 2016. Analysis of a 150 m sediment core from the coseismic subsidence depocenter of the 2009 Mw = 6.1 L'Aquila earthquake (Italy): implications for Holocene-Pleistocene tectonic subsidence rates and for the age of the seismogenic Paganica fault system, *Tectonophysics,* **687,** 180–194.

Malinverno, A. & Ryan, W.B.F., 1986. Extension in the Tyrrhenian Sea and shortening in the Apennines as result of arc migration driven by sinking of the lithosphere, *Tectonics,* **5**(2), 227–245.

Mancini, M., Cavuoto, G., Pandolfi, L., Petronio, C., Salari, L. & Sardella, R., 2012. Coupling infill history and mammal biochronology in a Pleistocene intramontane basin: the case of western L'Aquila Basin (central Apennines, Italy), *Quatern. Int.,* **267,** 62–77.

Mattson, A., 2004. Tomographic imaging of late Quaternary faulting, Oquirrh Mountains, Utah, *J. geophys. Res.,* **109,** B11310, doi:10.1029/2004JB003159.

Michetti, A.M., Brunamonte, F., Serva, L. & Vittori, E., 1996. Trench investigations of the 1915 Fucino earthquake fault scarps (Abruzzo, central Italy): geological evidence of large historical events, *J. geophys. Res.,* **101**(B3), 5921–5936.

Montone, P., Mariucci, M.T. & Pierdominici, S., 2012. The Italian present-day stress map, *Geophys. J. Int.,* **189,** 705–716.

Morewood, N.C. & Roberts, G.P., 2000. The geometry, kinematics and rates of deformation within an en echelon normal fault segment boundary, central Italy, *J. Struct. Geol.,* **22,** 1027–1047.

Morey, D. & Schuster, G.T., 1999. Paleoseismicity of the Oquirrh fault, Utah from shallow seismic tomography, *Geophys. J. Int.,* **138**(1), 25–35.

Moro, M., Bosi, V., Galadini, F., Galli, P., Giaccio, B., Messina, P. & Sposato, A., 2002. Analisi paleosismologiche lungo la faglia del M. Marine (alta valle dell'Aterno): risultati preliminari, *Il Quaternario (Ital. J. Quarter. Sci.),* **15,** 259–270.

Moro, M., Gori, S., Falcucci, E., Saroli, M., Galadini, F. & Salvi, S., 2013. Historical earthquakes and variable kinematic behaviour of the 2009 L'Aquila seismic event (central Italy) causative fault, revealed by paleoseismological investigations, *Tectonophysics,* **583,** 131–144.

Mouslopoulou, V., Walsh, J.J. & Nicol, A., 2009. Fault displacement rates on a range of timescales, *Earth planet. Sci. Lett.,* **278,** 186–197.

MS-AQ Working Group, 2010. Microzonazione sismica per la ricostruzione dell'area aquilana. Regione Abruzzo — Dipartimento della Protezione Civile, L'Aquila, 1–796 (in Italian). Available at: http://www.protezionecivile.gov.it/jcms/it/view_pub.wp?contentId=PUB25330, last accessed June 2016.

Nicol, A., Walsh, J.J., Watterson, J. & Underhill, J.R., 1997. Displacement rates of normal faults, *Nature,* **390,** 157–169.

Nicol, A., Walsh, J., Berryman, K. & Villarmor, P., 2006. Interdependence of fault displacement rates and paleoearthquakes in an active rift, *Geology,* **34**(10), 865–868.

Operto, S., Ravaut, C., Improta, L., Virieux, J., Herrero, A. & Dell'Aversana, P., 2004. Quantitative imaging of complex structures from dense wide-aperture seismic data by multiscale traveltime and waveform inversions: a case study, *Geophys. Prospect.,* **52,** 625–651.

Pace, B., Peruzza, L., Lavecchia, G. & Boncio, P., 2006. Layered seismogenic source model and probabilistic seismic-hazard analyses in Central Italy, *Bull. Soc. seism. Am.,* **96**(1), 107–132.

Pantosti, D., D'Addezio, G. & Cinti, F.R., 1996. Paleoseismicity of the Ovindoli-Pezza fault, central Apennines, Italy: a history including a large, previously unrecorded earthquake in the Middle Ages (860–1300 A.D.), *J. geophys. Res.,* **101**(B3), 5937–5959.

Patacca, E., Scandone, P., Di Luzio, E., Cavinato, G.P. & Parotto, M., 2008. Structural architecture of the central Apennines: interpretation of the CROP 11 seismic profile from the Adriatic coast to the orographic divide, *Tectonics,* **27**(3), doi:10.1029/2005TC001917.

Pelton, J.R., 2005. Near surface seismology: surface-base methods, in *Near-Surface Geophysics*, pp. 219–263, *Investigations in Geophysics*, Vol. 13, ed. Butler, D.K., Society of Exploration Geophysicists.

Podvin, P. & Lecomte, I., 1991. Finite difference computation of traveltimes in very contrasted velocity model: a massively parallel approach and its associated tools, *Geophys. J. Int.,* **105,** 271–284.

Pondrelli, S., Salimbeni, S., Ekström, G., Morelli, A., Gasperini, P. & Vannucci, G., 2006. The Italian CMT dataset from 1977 to the present, *Phys. Earth planet. Int.,* **159**(3–4), 286–303.

Porreca, M. *et al.*, 2016. Geological reconstruction in the area of maximum co-seismic subsidence during the 2009 Mw=6.1 l'Aquila earthquake using geophysical analyses and borehole stratigraphy, *Ital. J. Geosci.,* **135**(2), 350–362.

Pucci, S. *et al.*, 2015. Quaternary geology map of the Middle Aterno Valley, 2009 L'Aquila earthquake area (Abruzzi Apennines, Italy), *J. Maps,* **11**(5), 689–697.

Pucci, S. *et al.*, 2016. Deep Electrical Resistivity Tomography along the tectonically active Middle Aterno Valley (2009 L'Aquila earthquake area, central Italy), *Geophys. J. Int.,* **207,** 967–982.

Ravaut, C., Operto, S., Improta, L., Virieux, J., Herrero, A. & Dell'Aversana, P., 2004. Multiscale imaging of complex structures from multifold wide aperture seismic data by frequency-domain full-waveform tomography: application to a thrust belt, *Geophys. J. Int.,* **159,** 1032–1056.

Riguzzi, F., Crespi, M., Devoti, R., Doglioni, C., Pietrantonio, G. & Pisani, A.R., 2013. Strain relaxation of normal and thrust faults in Italy, *Geophys. J. Int.,* **195**(2), 815–820.

Roberts, G.P., 2006. Multi seismic cycle velocity and strain fields for an active fault system, *Earth planet. Sci. Lett.,* **251,** 44–51.

Roberts, G.P., Michetti, A., Cowie, P. A., Morewood, N.C. & Papanikolaou, I., 2002. Fault slip-rate variations during crustal-scale strain localisation, central Italy, *Geophys. Res. Lett.,* **29,** 9-1–9-4.

Roberts, G.P., Cowie, P., Papanikolou, I. & Michetti, A.M., 2004. Fault scaling relationships, deformation rates and seismic hazards: an example from the Lazio–Abruzzo Apennines, central Italy, *J. Struct. Geol.,* **26,** 377–398.

Roberts, G.P. *et al.*, 2010. Shallow subsurface structure of the 2009 April 6 Mw 6.3 L'Aquila earthquake surface rupture at Paganica, investigated with ground-penetrating radar, *Geophys. J. Int.,* **183,** 774–790.

Rovida, A., Camassi, R., Gasperini, P. & Stucchi, M. (eds), 2011. *CPTI11, the 2011 version of the Parametric Catalogue of Italian Earthquakes*. Milano, Bologna, last release 2011-12-23, http://emidius.mi.ingv.it/CPTI, doi:10.6092/INGV.IT-CPTI11.

Salvi, S., Cinti, F.R., Colini, L., D'Addezio, G., Doumaz, F. & Pettinelli, E., 2003. Investigation of the active Celano-L'Aquila fault system, Abruzzi (central Apennines, Italy) with combined ground-penetrating radar and paleoseismic trenching, *Geophys. J. Int.,* **155,** 805–818.

Scognamiglio, L., Tinti, E., Michelini, A., Dreger, D.S., Cirella, A., Cocco, M., Mazza, S. & Piatanesi, A., 2010. Fast determination of moment tensors and rupture history: what has been learned from the 6 April 2009 L'Aquila earthquake sequence, *Seismol. Res. Lett.,* **81** (6), 892–906.

Sheley, D., Crosby, T., Zhou, M., Giacoma, J., Yu, J., He, R. & Schuster, G.T., 2003. 2-D seismic trenching of colluvial wedges and faults, *Tectonophysics,* **368,** 51–69.

Spadi, M., Gliozzi, E., Cosentino, D. & Nocentini, M., 2015. Late Piacenzian-Gelasian freshwater ostracods (Crustacea) from the L'Aquila Basin (central Apennines, Italy), *J. System. Paleontol.,* **13**(11), 1–26.

Speranza, F. & Minelli, L., 2014. Ultrathick Triassic dolomites control the rupture behavior of the central Apennine seismicity: evidence from magnetic modeling of the L'Aquila fault zone, *J. geophys. Res.,* **119,** doi:10.1002/2014JB011199.

Stockwell, J.W., 1999. The CWP/SU: seismic Un*x package, *Comput. Geosci.,* **25**(4), 415–419.

Tavarnelli, E., 1999. Normal faults in thrust sheets: pre-orogenic extension, post-orogenic extension, or both?, *J. Struct. Geol.,* **21,** 1011–1018.

Tertulliani, A., Rossi, A., Cucci, L. & Vecchi, M., 2009. L'Aquila (Central Italy) earthquakes: the predecessors of the April 6, 2009 event, *Seismol. Res. Lett.,* **80**(6), 972–977.

Valensise, G. & Pantosti, D., 2001. The investigation of potential earthquake sources peninsular Italy: a review, *J. Seismol.,* **5**(3), 287–306.

Valoroso, L., Chiaraluce, L., Piccinini, D., Di Stefano, R., Schaff, D. & Waldhauser, F., 2013. Radiography of a normal fault system by 64,000 high-precision earthquake locations: the 2009 L'Aquila (central Italy) case study, *J. geophys. Res.,* **118,** 1156–1176.

Vezzani, L. & Ghisetti, F., 1998. Carta Geologica dell'Abruzzo, scale 1:100,000. S.EL.CA., Firenze.

Vezzani, L., Festa, A. & Ghisetti, F., 2010. Geology and tectonic evolution of the Central-Southern Apennines, Italy, *Geol. Soc. Am.,* Special Paper, 469, 58 pp.

Villani, F., Tulliani, V., Sapia, V., Fierro, E., Civico, R. & Pantosti, D., 2015a. Shallow subsurface imaging of the Piano di Pezza active normal fault (central Italy) by high-resolution refraction and electrical resistivity tomography coupled with time-domain electromagnetic data, *Geophys. J. Int.,* **203**(3), 1482–1494.

Villani, F. *et al.*, 2015b. Imaging the structural style of an active normal fault through multi-disciplinary geophysical investigation: a case study from the Mw 6.1, 2009 L'Aquila earthquake region (central Italy), *Geophys. J. Int.,* **200**(3), 1676–1691.

Vittori, E. *et al.*, 2011. Surface faulting of the 6 April 2009 M-w 6.3 L'Aquila Earthquake in Central Italy, *Bull. seism. Soc. Am.,* **101**(4), 1507–1530.

Wessel, P. & Smith, W.H.F., 1991. Free software helps map and display data, *EOS, Trans. Am. geophys. Un.,* **72**(41), 441–446.

Whittaker, A.C., Attal, M. & Allen, P.A., 2010. Characterising the origin, nature and fate of sediment exported from catchments perturbed by active tectonics, *Basin Res.,* **22**, 809–828.

Williamson, P.R. & Worthington, M.H., 1993. Resolution limits in ray tomography due to wave behaviour: numerical experiments, *Geophysic*s, **58**(5), 727–735.

SUPPORTING INFORMATION

Additional Supporting Information may be found in the online version of this paper:

Figure S1. Detail of CSG 51 of profile P2 (source $x = 567.5$ m; bandpass filter 30–100 Hz) plotted with reduction velocity of 4000 m s^{-1}: the red dashed line indicates a head wave from the top-basement and the green dashed line indicates a deep hypercritical reflection.

Figure S2. Selected CMP gathers of profile P2 showing deep basement reflections outlined by thin dashed green lines. The position of the reflection point corresponding to the 'zero offset' reflection (t_0) for each CMP gather is reported in the tomograms in Fig. 9 with a yellow star. Traveltimes t0 were depth-converted using average *Vp* values defined by refraction tomography (V_{tomo}). (a) cdp 106 ($x =$ 1828 m): t_0 0.12 s; (b) NMO correction (2400 m s^{-1}): top-basement depth –144 m (V_{tomo} 2300 m s^{-1}); (c) cdp 129 (x =1678 m): t_0 0.13 s; (d) NMO correction (2200 m s^{-1}): top-basement depth –143 m (V_{tomo} 2200 m s^{-1}); (e) cdp 194 ($x = 1608$): t_0 0.14 s; (f) NMO correction (2600 m s^{-1}): top-basement depth –182 m (V_{tomo} 2510 m s^{-1}); (g) cdp 296 ($x = 1348$ m): t_0 0.17 s; (h) NMO correction (2600 m s^{-1}): top-basement depth –221 m (V_{tomo} 2780 m s^{-1}); (i) cdp 475 ($x = 898$ m): t_0 0.16 s; (j) NMO correction (1900 m s^{-1}): top-basement depth –152 m (V_{tomo} 1900 m s^{-1}); (k) cdp 759 ($x =$ 188 m): t_0 0.2 s; (l) NMO correction (1800 m s^{-1}): top-basement

depth –180 m (V_{tomo} 1680 m s^{-1}); (m) cdp 656 ($x = 488$ m): t_0 0.24 s; (n) NMO correction (2400 m s^{-1}): top-basement depth –288 m (V_{tomo} 2270 m s^{-1}); (o) cdp 348 ($x = 1218$ m): t_0 0.19 s; (p) NMO correction (2600 m s^{-1}): top-basement depth –247 m (V_{tomo} 2600 m s^{-1}).

Figure S3. Selected CMP gathers of profile P1 showing deep basement reflections outlined by thin dashed green lines. The position of the reflection point corresponding to the 'zero offset' reflection (t_0) for each CMP gather is reported in the tomograms in Fig. 9 with a yellow star. Traveltimes t0 were depth-converted using average *Vp* values defined by refraction tomography (V_{tomo}). (a) cdp 73 ($x = 172$ m); t_0 0.125 s; (b) NMO correction (2400 m s^{-1}): top-basement depth –135 m (Vtomo 2175 m s^{-1}); (c) cdp 123 ($x = 312$ m); t_0 0.13 s; (d) NMO correction (1800 m s^{-1}): top-basement depth –143 m (Vtomo 2200 m s^{-1}); (e) cdp 183 ($x = 452$ m); t_0 0.18 s; (f) NMO correction (2200 m s^{-1}): top-basement depth –198 m (Vtomo 2290 m s^{-1}); (g) cdp 265 ($x = 662$ m); t_0 0.10 s; (h) NMO correction (1800 m s^{-1}): top-basement depth –116 m (Vtomo 2320 m s^{-1}); (i) cdp 327 ($x = 812$ m); t_0 0.115 s; (j) NMO correction (2100 m s^{-1}): top-basement depth –140 m (Vtomo 2430 m s^{-1}); (k) cdp 373 ($x = 937$ m (Vtomo 2320 m s^{-1}); (i) cdp 327 ($x = 812$ m); t_0 0.115 s; (j) NMO correction (2100 m s^{-1}): top-basement depth –140 m (Vtomo 2430 m s^{-1}); (k) m); t_0 0.07 s; (l) NMO correction (1800 m s^{-1}): top-basement depth –140 m (Vtomo 2430 m s^{-1}).
(http://gji.oxfordjournals.org/lookup/suppl/doi:10.1093/gji/ggw407/-/DC1)

Please note: Oxford University Press is not responsible for the content or functionality of any supporting materials supplied by the authors. Any queries (other than missing material) should be directed to the corresponding author for the paper.